

Northumbria Research Link

Citation: Malavolta, Marco, Costarelli, Laura, Giacconi, Robertina, Basso, Andrea, Piacenza, Francesco, Pierpaoli, Elisa, Provinciali, Mauro, Ogo, Ogo and Ford, Dianne (2017) Changes in Zn homeostasis during long term culture of primary endothelial cells and effects of Zn on endothelial cell senescence. *Experimental Gerontology*, 99. pp. 35-45. ISSN 0531-5565

Published by: Elsevier

URL: <https://doi.org/10.1016/j.exger.2017.09.006>
<<https://doi.org/10.1016/j.exger.2017.09.006>>

This version was downloaded from Northumbria Research Link:
<http://nrl.northumbria.ac.uk/32189/>

Northumbria University has developed Northumbria Research Link (NRL) to enable users to access the University's research output. Copyright © and moral rights for items on NRL are retained by the individual author(s) and/or other copyright owners. Single copies of full items can be reproduced, displayed or performed, and given to third parties in any format or medium for personal research or study, educational, or not-for-profit purposes without prior permission or charge, provided the authors, title and full bibliographic details are given, as well as a hyperlink and/or URL to the original metadata page. The content must not be changed in any way. Full items must not be sold commercially in any format or medium without formal permission of the copyright holder. The full policy is available online: <http://nrl.northumbria.ac.uk/policies.html>

This document may differ from the final, published version of the research and has been made available online in accordance with publisher policies. To read and/or cite from the published version of the research, please visit the publisher's website (a subscription may be required.)

www.northumbria.ac.uk/nrl



Highlights

- Chronic exposure to a moderately high dose of Zn accelerates senescence in human primary endothelial cells
- Senescent endothelial cells display altered Zn homeostasis and increased expression of genes involved in protection against Zn toxicity
- Senescent endothelial cells undergo partial cell death in response to short-term treatment with a high dose of Zn
- Senescent endothelial cells acquire resistance to Zn depletion, which may underline a potential pathological mechanism related to Zn deficiency

Title

Changes in Zn homeostasis during long term culture of primary endothelial cells and effects of zinc on endothelial cell senescence

Running Title: Zn homeostasis and endothelial senescence

Marco Malavolta¹, Laura Costarelli¹, Robertina Giacconi¹, Andrea Basso¹, Francesco Piacenza¹, Elisa Pierpaoli¹,
Mauro Provinciali¹, Ogo A Ogo², Dianne Ford³

Affiliations:

1: Nutrition and Aging Centre, INRCA, Italy

2: Institute for Cell and Molecular Biosciences, University of Newcastle, Newcastle upon Tyne, UK

3: Faculty of Health and Life Sciences, Northumbria University, Newcastle upon Tyne, UK

Address for correspondence and reprints:

Dr Marco Malavolta, PhD (Current position: Contract Researcher)

E-mail: m.malavolta@inrca.it

Phone: 0039-0718004116

Abstract

Endothelial cell senescence and Zn nutritional status influence cardiovascular disease. The influence of Zn appears dichotomous, hence it is imperative to understand the relationship with cellular senescence to improve knowledge about the molecular and cellular basis of the disease. Here we aimed to determine: 1) the impact of chronic exposure to a moderately high dose of Zn on senescence of endothelial cells; 2) the changes in Zn homeostasis during the lifespan of primary cultured endothelial cells; 3) the susceptibility of proliferating and senescent endothelial cells to cell death after short term exposure to increasing doses of Zn and of the Zn chelator TPEN. Chronic exposure to Zn accelerated senescence and untreated cells at later passages, where doubling time had increased, displayed relocation of labile Zn and altered expression of genes involved in the response to Zn toxicity, including SLC30A1, SLC39A6, SLC30A5, SLC30A10 and metallothioneins, indicating that senescent cells have altered zinc homeostasis. Most Zn-dependent genes that were expressed differently between early and late passages were correlated with changes in the expression of anti-apoptotic genes. Short-term treatment with a high dose of Zn leads to partial cell death, but only in the population of cells at both earlier and later passages that had already entered senescence. In contrast, Zn depletion led to death of cells at earlier but not later passages, which suggests that there are sub-populations of senescent cells that are resistant to Zn depletion. This resistant senescent cell population may accumulate under conditions of Zn deficiency and contribute to vascular pathology.

Keywords: Cellular Senescence, Zn homeostasis, p16, Zn transporters, labile Zn, aging

Introduction

Endothelial cell senescence plays a role in human aging and age-related vascular disorders. Senescent endothelial cells are present in human atherosclerotic lesions (Minamino et al., 2002), where they are likely to promote pathology (Childs et al., 2016; Fyhrquist et al., 2013; Krouwer et al., 2012). Both transgenic and pharmacological approaches to clear senescent cells have provided preclinical evidence that selective ablation could contribute to the development of new therapeutic approaches to treating cardiovascular disease (Childs et al., 2016; Soto-Gamez and Demaria, 2017). However, to date few compounds able to selectively ablate senescent cells (senolytic drugs) are known, and they are not effective in all senescent cell types (Soto-Gamez and Demaria, 2017).

Why senescent cells accumulate in tissues and organs with age is still a key open question. Accumulation of senescent cells in aged tissues may be driven by several factors including an increased rate of formation of senescent cells, loss of senescence immunosurveillance, bystander effects caused by secretory phenotype on neighbouring cells and upregulation of intrinsic anti-apoptotic factors (van Deursen, 2014). Since Zn ions are important mediators of apoptotic pathways, and can both enhance or repress functional apoptosis (Garufi et al., 2016; McCabe et al., 1993; Perry et al., 1997; Truong-Tran et al., 2000; Zalewski et al., 1994), manipulating the exposure of cells to Zn may be an effective strategy to modulate cell senescence or to promote the death of senescent cells. In support of this idea, quercetin, a natural polyphenol and Zn ionophore (Dabbagh-Bazarbachi et al., 2014), induced selective death of senescent endothelial cells over proliferating cells (Zhu et al., 2015). Moreover, dysregulated Zn balance has been shown to induce senescence in dermal fibroblasts (Rudolf and Cervinka, 2011) and the Zn ionophore pyrithione was identified as a senescence-inducing compound in a screen of 4160 compounds (Ewald et al., 2009). Zn deficiency is considered a risk factor for the development of atherosclerosis (Beattie and Kwun, 2004), but the cellular and molecular basis of this association has not been investigated in depth. We propose that the influence of Zn on endothelial cell senescence makes an important contribution to this observation. Since impaired Zn homeostasis is a feature of older age, we also propose that altered Zn homeostasis in senescent compared with replicating endothelial cells is an interacting influence.

Commensurate with this idea, experiments performed in a vascular smooth muscle cell model suggest that cellular senescence is a Zn-dependent mechanism driven by specific Zn transporters involved in the regulation of intracellular Zn ions (Patrushev et al., 2012). The complex homeostatic network to which these transporters belong includes members of two families of Zn transporters, which together comprise 24 genes (Cousins et al., 2006; Lichten and Cousins, 2009), metallothioneins (MTs) (Mocchegiani et al., 2013), and Zn sensors (ZNF658 and MTF-1) (Choi and Bird, 2014; Ogo et al., 2015).

The purpose of this study was to investigate: 1) the impact of chronic treatment with a moderate excess of Zn on Zn content and distribution and on replicative potential and senescence in human coronary artery endothelial cells (HCAECs); 2) changes in Zn homeostasis over the lifespan of endothelial cells, using passage number as a surrogate for senescence, using transcriptomic data from two endothelial cell models (HCAECs and Human Umbilical Vein Endothelial Cells-HUVECs); 3) the impact of Zn and passage number on the expression of major players in Zn homeostasis over the culture lifespan of HCAECs; 4) the susceptibility to cell death induced by increasing doses of Zn or of the Zn chelator TPEN at early and later passages of HCAECs.

Material and Methods

Cell culture

HCAECs (Human coronary artery endothelial cells) were purchased from Clonetics Corporation (Lonza) and cultured in endothelial basal medium EBM, supplemented with EGM-2/MV SingleQuots with or without addition of 50 μ M ZnSO₄. This concentration has been already defined by others as moderately excessive and does not have a significant effect on the growth or morphology of endothelial cells (Bobilya et al., 2008). HCAECs were plated at a seeding density of 2,500 cells/cm² in T 25 flasks and passaged serially. Harvested cells were counted using the Trypan blue viability stain. Population doublings (PD) were calculated using the formula $(\log_{10}UCY - \log_{10}I) \times 3.32$ (where UCY is the number of cells at the end of the passage and I is the number of cells initially seeded). Cells were collected for immediate assessment by flow cytometry or for RNA extraction for subsequent 4

analysis of gene expression. Total RNA was extracted from HCAECs using the RNeasy Mini Kit (Qiagen, Hilden, Germany), according to the manufacturer's instructions. RNA concentration and purity were measured using a NanoDrop spectrometer and samples were stored at -80 °C for measurement using RT-PCR.

Senescence biomarkers

HCAECs were grown for subsequent passages until two consecutive population doublings equal to or below 0 were achieved, associated with morphological changes indicating senescence revealed by microscopy and flow cytometry. Cumulative population doubling (CPD) was calculated as the sum of all population doublings (PDs). Senescence associated beta-galactosidase activity (SA- β -gal) was measured by flow cytometry as described previously (Noppe et al., 2009). As an additional biomarker of senescence, p16 mRNA levels were measured by real-time RT-PCR. Positive staining with propidium iodide was used as the marker of cell viability.

Measurement of labile Zn and metallothionein protein

Labile Zn was measured by flow cytometry using the membrane permeable Zn specific probe FluoZin-3-AM (Haase et al., 2006). Localization of fluorescence after staining endothelial cells with the membrane permeable Zn probe and LysoTracker red (ThermoFischer Scientific) was detected by imaging flow cytometry (Flowsight, Amnis Corporation, Seattle, WA, USA), as described previously for brain endothelial cells (Lopes Pinheiro et al., 2016). Briefly, cells were acquired on the basis of their area. Analysis was performed with a 488 nm laser line on single cells after compensation. The relative level of co-localization was calculated using the bright detail similarity feature R3 in the Ideas v6.0 software (Amnis-Merck Millipore). This feature corresponds to the logarithmic transformation of Pearson's correlation coefficient of the localized bright spots with a radius of 3 pixels or less within the whole cell area in the two input images. Labile Zn spots marked by FluoZin-3 were calculated using the spot count feature of the Ideas software.

Metallothionein protein expression was measured by flow cytometry following a previously-established protocol (Malavolta et al., 2008, 2007, 2006). Briefly: cells were incubated with the MT-specific monoclonal antibody (1

$\mu\text{g}/10^5$ cells/200 μl) (monoclonal mouse anti-horse metallothionein clone E9, from DAKOCYTOMATION, Denmark) for 30 min at room temperature. Following treatment with the primary antibody, the cells were washed with staining buffer and incubated for 1 h at room temperature with a FITC-conjugated secondary antibody (goat anti mouse Ig, Becton Dickinson, USA). MT-specific fluorescence (MFI) of the sample was determined by subtracting the mean fluorescence intensity obtained with the isotypic antibody clone MOPC21, IgG1k, (Sigma-Aldrich, St. Louis, USA) from the one obtained with the MT-specific antibody.

Quantitative reverse transcription polymerase chain reaction (qRT-PCR)

cDNA synthesis from total RNA was performed using i-Script reverse transcriptase (Biorad, Hercules, CA) according to the manufacturer's guidelines. Messenger RNA for β -actin and GAPDH (glyceraldehyde-3-phosphate dehydrogenase) reference genes and for p16, SLC30A1, SLC39A6, SLC39A1, SLC39A2, SLC39A3, SLC30A5, SLC30A10, CBWD, ZNF658, MT2A, MT1X and MT1F was then measured by real-time PCR on a BioRad iQ5 optical realtime thermal cycler (Biorad, Hercules, CA) using 1 μg of cDNA in a total volume of 25 μl containing iQ SYBR Green Supermix (Biorad, Hercules, CA). Primer sequences and thermal cycling parameters for SLC30A5, SLC30A10, CBWD, and GAPDH were as specified previously (Coneyworth et al., 2012). The other primers used are listed in **Supplementary Table 1**. Primer concentrations of 200 nM were used for MT1X, MT2A, SLC30A1, ZNF658, SLC39A3 and SLC309A6 genes; 150 nM for p16 and β -ACTIN, and 300 nM for MT1F and SLC39A2 genes. Assays for each transcript were carried out as duplicates. Fold changes relative to the control condition at the earliest passage were calculated using the $\Delta\Delta\text{Ct}$ method. β -actin was used as the reference gene for p16. GAPDH was used as the reference gene for the other mRNAs measured. Data are compared to the control condition at the earliest passage.

Whole genome expression analysis

Data were obtained using the GeneChip 3' IVT Express kit (Affymetrix, Santa Clara, CA, USA). An integrated meta-analysis of the original *.CEL files was performed using Partek Genomic Suite Software v6.6 (Partek inc.) and

from 3 replicates each of HuVECs and HCAECs harvested at early and late passages (passages 4 and 18 for HuVECs; passages 6 and 12 for HCAECs). For statistical analysis, we first identified genes significantly ($p < 0.05$ and $FDR < 0.05$) upregulated and downregulated in late compared with early-passage cells (both HUVEC and HCAEC) using the ANOVA tool integrated in the Partek Genomic Suite. Those genes in this list known to regulate Zn homeostasis were selected for cluster analysis. We also imported probesets data in SPSS v. 22 (IBM) and performed principal component analysis using all probesets tagged to Zn transporters, MTs and metal transcription factors. Correlation between the functions identified through this analysis and genes believed to promote survival in senescent cells was also determined. Comparison among experimental groups for labile Zn and other data acquired using targeted (as opposed to transcriptome-wide) measurements was performed using a mixed models tool for repeated measures in SPSS v. 22 (IBM). In order to take into account eventual unbalanced data, we set build options with Satterthwaite approximation and used robust estimation to handle violations of model assumption. Post-hoc comparisons were performed by LSD.

Results

Growth and replicative senescence of control and Zn-treated HCAEC cultures

To determine if the presence of Zn (50 μM) in the medium affects the growth, survival and replicative senescence of HCAECs, cells were subjected to serial passage and growth was monitored in Zn-supplemented and control medium by examining replicative capability over the culture lifespan. Regardless of treatment with Zn, cells appeared to undergo growth arrest after passage nine (**Fig. 1 - Panel A** and **Tab. 1**). However, growth arrest in Zn-treated cells was accelerated compared with control cells, suggesting that Zn stimulated transition to senescence. We observed a decline in cell viability in the later passages, which is a usual observation when culturing primary human endothelial cells (Unterluggauer et al., 2003; Wagner et al., 2001). Notably, cell viability was higher in control cells compared with Zn-treated cells after passage 9 (**Tab. 1**). Almost all Zn-treated cells (approximately 90%) had undergone cell death by passage 11, whereas only approximately 40% of control cells

had undergone cell death by this point. Measurement of SA- β -gal staining and p16 expression as biomarkers of senescence revealed increases induced by the Zn treatment at late passages (**Fig. 1 – Panels B and C**).

Effects of passage number and Zn treatment on Zn content and distribution and on morphology of HCAECs

To determine if Zn-induced senescence is accompanied by changes in labile Zn in endothelial cells, we performed flow cytometric measurements of labile Zn using the probe FluoZin3-AM during serial passage of Zn-treated and control HCAECs. We additionally characterised two distinct sub-populations of cells (**Fig. 2**). These two gates represent two populations discriminated by forward and side scatter that have some features, respectively, of replicating and senescent cells. We refer hereafter to the sub-population that features larger cells (revealed by forward scatter) and granularity (revealed by side scatter) as the “Large-HCAEC” (L-HCAEC) sub-population. This sub-population increases as a proportion of the total cell number with increasing CPDs and Zn treatment (**Fig. 2 – Panel C**) and in later passages includes more cells that are highly positive for SA- β -gal (**Suppl. Fig. 1**). We refer to the smaller, less granular sub-population of cells that are predominant in rapidly replicating passages as the “non-Large-HCAEC” (nL-HCAEC) sub-population. Representative examples of histograms obtained with FluoZin3 in these 2 gates are shown in **Fig. 2 (Panels D and E)**. The measurement of intracellular labile Zn was performed after estimating minimum and maximum fluorescence with TPEN and pyrithione, respectively (Haase et al., 2006).

Zn appears to be positively correlated with CPDs in ungated cells as well as in nL-HCAEC and L-HCAEC sub-populations. (**Fig. 3**). When we grouped cells by CPDs as early (1-6 CPDs), medium (7-11 CPDs) and late (> 11 CPDs), we observed a significant increase in labile Zn in untreated HCAECs at late CPDs compared with the other two groups (**Fig. 3, panel D and E**) and this change was accelerated by Zn treatment. Moreover, labile Zn levels were increased in the L-HCAEC compared with nL-HCAEC sub-population at early ($p < 0.01$), middle ($p < 0.01$) and late ($p < 0.05$) CPDs (**Fig. 3 panel E** in comparison to **Fig. 3 panel D**). Zn treatment significantly increased the

levels of labile Zn in both sub-populations. Labile Zn in L-HCAEC was higher than the respective measurement performed in the nL-HCAEC gate.

Imaging flow cytometry confirmed the higher FluoZin-3 signal in the senescence-enriched L-HCAEC sub-population at later passages (**Suppl. Fig. 2, Panels a, b and c**). Many cells displayed punctuate fluorescent spots, which were at higher numbers in the L-HCAEC sub-population compared with the nL-HCAEC sub-population (**Suppl. Fig. 2, Panel d**) but at lower numbers in the L-HCAEC sub-population at later compared with earlier passages (**Suppl. Fig. 2, Panels d, e, f**). Morphological analysis of FluoZin-3 fluorescence revealed that this apparent loss of fluorescent spots at later passages in the L-HCAEC sub-population was compensated by a diffused fluorescence (**Suppl. Fig. 2 Panels g and h**). Since an expansion of the lysosomal compartment is a feature of senescent cells, we predicted that the increased labile Zn at later passage numbers was located in this compartment. Commensurate with the fluorescent spots being lysosomes and the more diffused fluorescence being Zn in a different subcellular location, Lysotracker signal intensity was increased at higher passage numbers (**Fig. 4, Panels a, b and c**) but its colocalization with FluoZin-3 decreased in the L-HCAEC compared with nL-HCAEC sub-population and at later compared with earlier passages of the L-HCAEC sub-population (**Fig. 4, Panels d-h**).

Expression of Zn regulating genes in HCAECs and HUVECs at earlier and later passages revealed by analysis of transcriptomic data

To gain further insight into the relationship between Zn homeostasis and endothelial cell senescence we compared transcriptomes at early and late passages in two different endothelial cell lines (HCAEC and HUVEC) to determine commonalities and eliminate responses that are cell-line specific. Data from HCAECs were from our published work that compared passage 6 with passage 12 (GEO accession number GSE77239) (Costarelli et al., 2017). Data from HUVECs were from were from a study that compared cells at passage 4 with cells at passage 18 (GEO accession number GSE13712) (Mun et al., 2009). The workflow of this study is presented as **Supplementary Figure 3**. In HUVECs, 7469 probesets were expressed differently (3227

downregulated) in the earlier compared with the later passage while in HCAECs 11897 probesets were expressed differently (5180 up- and 6717 downregulated) in the earlier compared with the later passage. Merged analysis identified 4140 probesets (2008 up and 2132 downregulated) expressed differently in endothelial cells at earlier compared with later passages. Nine of these probesets (for a total of 5 genes - SLC30A1, SLC39A6, MTF1, SLC39A13, SLC39A7) were involved in Zn homeostasis and showed a similar response (direction of change) in HCAECs and HUVECs (**Table 2**). Other players in Zn homeostasis were differently expressed between the earlier and later passage in only one of the two endothelial cell lines (**Suppl. Tab. 2 and 3**). Cluster analysis of these genes clearly discriminated endothelial cells at later versus earlier passages (**Suppl. Fig. 4**). All probesets tagged to genes known to regulate Zn homeostasis were also used for principal component analysis, which generated two functions, PCA1 and PCA2 (**Suppl. Tab. 4**), that significantly discriminate cell type and early/late passage, respectively (**Suppl. Fig. 5**). PCA2 was positively correlated with probesets tagged to Zn exporters (SLC30A1), intracellular importers (SLC30A5, SLC30A6), Zn sensors (MTF1) and MT genes, thus suggesting a strict relationship with Zn mobilization. Correlation of PCA2 with genes selected from the transcriptome data that are known to regulate apoptosis in senescent cells (**Suppl. Tab. 5**) (Zhu et al., 2015) identified at least 4 genes associated with intracellular Zn mobilization (BCL2L1, SERPINE2, CDKN1A and ABL1). Other genes highly correlated with PCA2 ($r > 0.865$ and $p < 0.001$) and significantly affected by endothelial cell passage number (in total 117 genes) included several genes known to be involved with cell cycle arrest (CDKN2A, CDKN2C, CCNA1, CENPA, CDKN2C, FOXM1, NEK6) and cell adhesion (ICAM1, CLDN1, CECAM1, PLAUR) (**Suppl. Tab. 6**).

Expression of targeted Zn regulating genes during growth of control and Zn-treated HCAECs

We reasoned that the changes in labile Zn in HCAECs as CPDs increased would be manifest as an altered response of Zn-sensitive genes to Zn. Thus, we measured the response to Zn at different CPDs of a panel of genes identified primarily from the transcriptomic data. These included common genes significantly different in later compared with earlier passages of HCAECs and HUVECs (SLC30A1, SLC39A6), a subset of genes that characterized PCA2 (SLC30A5, SLC39A1, MT2A, MT1X, MT1F) and additional genes known to be modulated by Zn or by Zn regulated 10

transcriptional factors (SLC30A10, SLC39A2, SLC39A3, CBWD, ZNF658). As we predicted, the response to Zn differed between cells grouped as early CPDs versus late CPDs for specific genes in this panel – ZnT10, MT2A and MT1F - as shown through a significant interaction between Zn and CPD revealed by statistical analysis (mixed models for repeated measures) (**Fig. 5**).

When we included all gene expression data in a model of automatic regression versus p16 expression we identified the ratio between ZNF658 to SLC30A10 as the most important predictor (**Suppl. Fig. 6, Panel A**).

Metallothionein protein expression

While MT mRNAs were found to be only slightly affected by senescence in the HCAEC model we investigated if protein expression followed a similar pattern. Protein expression of MTs was found to be downregulated in late CPDs of both treated and untreated cells (**Suppl. Fig. 7**).

Effect of acute treatment with increasing doses of Zn and TPEN in proliferating and senescent cells

The altered Zn homeostasis observed in endothelial cells at later passages led us to investigate if senescent HCAECs and/or HCAECs at later passages are more susceptible to death (measured by propidium iodide) induced by an acute treatment with increasing doses of Zn or of the Zn chelator TPEN. For this purpose, we used samples of cells with a viability higher than 75%. With this criterion, we excluded potential bias due to the occurrence of death processes in HCAEC after passage 10. Treatment with TPEN for 48h in cells at an earlier passage (passage 5), decreased viability at concentrations of 100 and 500 nM in both nL-HCAEC and L-HCAEC sub-populations compared with untreated cells (**Fig. 6, Panel A**). Treatment of cells at the earlier passage with Zn (as ZnSO₄) induced a decrease in viability at concentrations of 100 and 150 μM exclusively in the L-HCAEC sub-population (**Fig. 6, Panel B**). This observation indicates that the few HCAECs with high Zn staining and morphological features of senescent cells that are present in early passages (around 5% of the whole cell population, as displayed in **Fig. 2**) are more susceptible than proliferating cells to death induced by high Zn. Surprisingly, none of the TPEN doses

induced significant evidence of cell death in either sub-population of cells at a higher passage number (passage

10; **Fig. 6, Panel C**). This observation leads us to suggest that there are further sub-divisions of both L-HCAEC and nL-HCAEC sub-populations that are resistant to zinc depletion that increase in proportion at higher passage numbers. The response to Zn of cells at the higher passage number was the same as at the lower passage number; only the senescence-enriched L-HCAEC sub-population showed a significant loss of viability (**Fig. 6, Panel D**). We interpret this pattern of response to Zn as revealing that replicating endothelial cells must first pass through the senescent state to be killed by excess Zn.

Discussion

We provide evidence that Zn promotes the entry of HCAECs into senescence, and that senescent HCAECs show disrupted Zn homeostasis, which may be related to the susceptibility of senescent cells to undergo cell death in response to Zn treatment. We also show that Zn depletion leads to death of only young, replicating cells.

Acceleration of entry into senescence by Zn was shown as accelerated growth arrest and through an observation that Zn increases the proportion of larger cells, detected using flow cytometry, that have features of senescent cells, including expression of the senescence markers SA- β -gal and p16. Labile Zn, measured using FluoZin-3, increased over the culture lifespan of HCAECs and was higher in the senescence-enriched, larger cell sub-population (L-HCAEC sub-population).

As expected, the lysosomal compartment, revealed by staining with LysoTracker dye, increased at later passages. However, the higher Zn content was not accommodated entirely within lysosomes, as revealed by reduced co-localization of FluoZin-3 and LysoTracker signals. Zn in the cytoplasm or other compartments may play a role in the synthesis of Zn dependent proteins of the senescence associated secretory phenotype (SASP) as well as in other aspects of the senescent cell phenotype (Pantsulaia et al., 2016). Since intracellular labile Zn is an important element of the cellular stress response, cellular metabolic activity and synthesis of proteins (Beyersmann and Haase, 2001), the changes observed may reflect increased proteotoxic stress as a consequence of the SASP (Coppé et al., 2010; Dörr et al., 2013). In senescent vascular smooth muscle cells, it has been reported that 12

mitochondria are sites of accumulation of Zn and that this phenomenon is related to an increase in the production of reactive oxygen species (ROS) (Salazar et al., 2017).

Altered Zn homeostasis was evident as changes in gene expression at later passages of HCAECs, as well as through these changes in Zn content and distribution. The players in Zn homeostasis that were found to be altered at later stages in the culture lifespan included genes that are responsive to Zn treatment and that normally act to protect cells against Zn toxicity. These included SLC30A1, SLC39A5, SLC30A6, SLC30A10 and MTs. Notably, SLC30A10 and SLC30A5 are both under the control of ZNF658 (Ogo et al., 2015) and the ZNF658 to SLC30A10 mRNA ratio was highly correlated with the mRNA of the senescence marker p16, suggesting that the component of the Zn-homeostatic machinery regulated by ZNF658 may be particularly pivotal in the transition between endothelial cell replication and senescence. In concordance with this proposal, the Zn transcriptional regulatory element (ZTRE), which mediates the effect of ZNF658 on gene transcription, was identified in at least 3 genes (HSPA9, RAD51 and NOS3) (Coneyworth et al., 2012) that are known to counteract cellular senescence (Rodier et al., 2011; Xiao-Hong et al., 2013; Yaguchi et al., 2007). These findings concur with observations made in vascular smooth muscle cells, where cellular senescence was found to be mediated by downregulation of SLC30A10 (as well as SLC30A3) (Patrushev et al., 2012). The data do not allow us to disentangle cause and effect with respect to which changes in expression of the Zn homeostatic machinery may drive cells into senescence and which are consequences of the ensuing Zn-dyshomeostasis. It is likely that these interactions are complex, and that several Zn-responsive genes, including Zn transporters, rather than a single 'trigger' gene, contribute to promoting senescence. Determining if overexpression or knockdown of individual Zn transporters in cells at later passages reverses the senescent phenotype would be informative in this context.

Overall our results are consistent with an upregulation of Zn responsive genes in senescent endothelial cells with the notable exception of MT mRNAs in the HCAEC model, which were unaltered (MT1X and MT2A) or slightly reduced (MT1F) in the absence of Zn treatment. MT protein was also slightly reduced. The nature of this dichotomy is still not completely explained, but may be a consequence of increased oxidative stress in senescent 13

endothelial cells (Donato et al., 2015) and the increased propensity for oxidized and apo-MTs that have released Zn in response to be degraded (Klaassen et al., 1994). We have previously observed a similar phenomenon in late passages of T cell clones (Malavolta et al., 2008). We observed that HCAECs at later passages nonetheless retained the capacity for Zn to induce MTs, specifically MT2A and MT1F.

On the basis of the perturbed Zn homeostatic response we observed in endothelial cells at later passages, we predicted that cells would be more susceptible to cell death induced by using TPEN to deplete Zn or to Zn excess at later passages. However, we found that cells at an earlier passage (passage 5) were more susceptible to death induced by TPEN than were cells at a later passage (passage 10), and that this observation applied to both the nL-HCAEC and L-HCAEC sub-populations. We interpret this observation as revealing that there are further sub-divisions of both sub-populations (shown schematically in **Fig. 7**) that are resistant to zinc depletion and that these increase in proportion at higher passage numbers. Resistance to death by apoptosis is a feature of senescent cells. Thus, these findings concur with this paradigm. The range of doses of TPEN applied were 20 to 500 times lower than the TPEN concentration (10 μ M) that is used to completely deplete Zn from cells (Seve et al., 1999). Hence, the level of Zn depletion achieved is likely to be commensurate with depleted levels that can be observed in human plasma. We posit that the (large) senescent sub-population of these persistent cells may contribute to the reported association between atherosclerosis and Zn deficiency (Chen et al., 2016; Tomat et al., 2011) and may increase disease risk under conditions of impaired Zn homeostasis and depleted plasma Zn concentration, for example in older age.

We observed no difference in the response to chronic exposure to high concentrations of Zn between cells at the earlier and later passage. Only the senescence-enriched L-HCAEC sub-population at both points in the replicative lifecycle showed a significant loss of viability. We interpret this pattern of response to show that replicating endothelial cells must first pass through the senescent state to be killed by excess Zn (shown schematically in **Fig 7**). In these experiments, we exceeded by 10 times the concentration in human plasma (around 15 μ M). Concentrations of this order would not be achievable in the plasma because homeostatic 14

mechanisms are invoked to maintain relatively stable plasma Zn levels. However, we did not aim to mimic conditions that may be achievable in vivo. Our aim was to apply a maximal challenge to the endothelial intracellular Zn homeostatic processes to probe the relationship between Zn and endothelial cell senescence and death. Our finding that senescence might precede cell death even under such an extreme Zn challenge makes this finding particularly robust. The Zn response function (PCA2) identified by principal component analysis of gene expression differences between early and later passages of endothelial cells was correlated with the expression of genes known to regulate apoptosis in senescent cells. Hence, it is likely that the addition of Zn may accelerate the activation of these pathways and contribute to the death observed in the senescence-enriched sub-population. This retained sensitivity to death induced by acute Zn toxicity is converse to the known resistance to apoptosis of senescent cells, but concurs with retained sensitivity to death induced by Zn we observed over chronic exposure to the lower (50 μ M) dose and is supportive of our proposal that Zn dyshomeostasis in senescent cells would render them sensitive to death induced by Zn.

Conclusions

In conclusion, chronic exposure to a moderately high dose of Zn accelerates senescence in HCAECs. Senescent HCAECs display altered Zn homeostasis characterized by intracellular relocation of Zn, and endothelial cells at later passages show increased expression of several genes involved in protection against Zn toxicity. Only senescent HCAECs undergo partial cell death in response to short-term treatment with a high dose of Zn. Both replicating cells and cells with senescent-like morphology (L-HCAEC gate) are killed by Zn depletion at earlier passages, but senescent cells acquire resistance to Zn depletion at later passages, which may underline a potential vascular pathological mechanism related to the accumulation of harmful senescent endothelial cells under conditions of Zn deficiency or systemic Zn-dyshomeostasis.

Acknowledgements

The present study was supported by the FA COST Action TD1304, The Network for the Biology of Zn (Zn-Net), research grant BB/F019637/1 (to DF) from the UK Biotechnology and Biological Sciences Research Council (BBSRC) and by the Tertiary Education Trust Fund through the Benue State University (BSU), Makurdi, Nigeria (PhD studentship to OAO).

Author Disclosure Statement

The authors declare no conflict of interest.

References

Beattie, J.H., Kwun, I.-S., 2004. Is zinc deficiency a risk factor for atherosclerosis? *Br. J. Nutr.* 91, 177.

doi:10.1079/BJN20031072

Beyersmann, D., Haase, H., 2001. Functions of zinc in signaling, proliferation and differentiation of mammalian cells. *Biometals* 14, 331–41.

Bobilya, D.J., Gauthier, N.A., Karki, S., Olley, B.J., Thomas, W.K., 2008. Longitudinal changes in zinc transport kinetics, metallothionein and zinc transporter expression in a blood-brain barrier model in response to a moderately excessive zinc environment. *J. Nutr. Biochem.* 19, 129–37. doi:10.1016/j.jnutbio.2007.06.014

Chen, J., Wang, S., Luo, M., Zhang, Z., Dai, X., Kong, M., Cai, L., Wang, Y., Shi, B., Tan, Y., 2016. From the Cover: Zinc Deficiency Worsens and Supplementation Prevents High-Fat Diet Induced Vascular Inflammation, Oxidative Stress, and Pathological Remodeling. *Toxicol. Sci.* 153, 124–136. doi:10.1093/toxsci/kfw110

Childs, B.G., Baker, D.J., Wijshake, T., Conover, C.A., Campisi, J., van Deursen, J.M., 2016. Senescent intimal foam cells are deleterious at all stages of atherosclerosis. *Science* 354, 472–477.

doi:10.1126/science.aaf6659

- Choi, S., Bird, A.J., 2014. Zinc'ing sensibly: controlling zinc homeostasis at the transcriptional level. *Metallomics* 6, 1198. doi:10.1039/c4mt00064a
- Coneyworth, L.J., Jackson, K.A., Tyson, J., Bosomworth, H.J., van der Hagen, E., Hann, G.M., Ogo, O.A., Swann, D.C., Mathers, J.C., Valentine, R.A., Ford, D., 2012. Identification of the human zinc transcriptional regulatory element (ZTRE): a palindromic protein-binding DNA sequence responsible for zinc-induced transcriptional repression. *J. Biol. Chem.* 287, 36567–81. doi:10.1074/jbc.M112.397000
- Coppé, J.-P., Desprez, P.-Y., Krtolica, A., Campisi, J., 2010. The senescence-associated secretory phenotype: the dark side of tumor suppression. *Annu. Rev. Pathol.* 5, 99–118. doi:10.1146/annurev-pathol-121808-102144
- Costarelli, L., Giacconi, R., Malavolta, M., Basso, A., Piacenza, F., Provinciali, M., Maggio, M.G., Corsonello, A., Lattanzio, F., 2017. Different transcriptional profiling between senescent and non-senescent human coronary artery endothelial cells (HCAECs) by Omeprazole and Lansoprazole treatment. *Biogerontology* 18, 217–236. doi:10.1007/s10522-016-9675-3
- Cousins, R.J., Liuzzi, J.P., Lichten, L.A., 2006. Mammalian zinc transport, trafficking, and signals. *J. Biol. Chem.* 281, 24085–9. doi:10.1074/jbc.R600011200
- Dabbagh-Bazarbachi, H., Clergeaud, G., Quesada, I.M., Ortiz, M., O'Sullivan, C.K., Fernández-Larrea, J.B., 2014. Zinc Ionophore Activity of Quercetin and Epigallocatechin-gallate: From Hepa 1-6 Cells to a Liposome Model. *J. Agric. Food Chem.* 62, 8085–8093. doi:10.1021/jf5014633
- Donato, A.J., Morgan, R.G., Walker, A.E., Lesniewski, L.A., 2015. Cellular and molecular biology of aging endothelial cells. *J. Mol. Cell. Cardiol.* 89, 122–135. doi:10.1016/j.yjmcc.2015.01.021
- Dörr, J.R., Yu, Y., Milanovic, M., Beuster, G., Zasada, C., Däbritz, J.H.M., Lisec, J., Lenze, D., Gerhardt, A., Schleicher, K., Kratzat, S., Purfürst, B., Walenta, S., Mueller-Klieser, W., Gräler, M., Hummel, M., Keller, U.,

Buck, A.K., Dörken, B., Willmitzer, L., Reimann, M., Kempa, S., Lee, S., Schmitt, C.A., 2013. Synthetic lethal metabolic targeting of cellular senescence in cancer therapy. *Nature* 501, 421–5.

doi:10.1038/nature12437

Ewald, J.A., Peters, N., Desotelle, J.A., Hoffmann, F.M., Jarrard, D.F., 2009. A high-throughput method to identify novel senescence-inducing compounds. *J. Biomol. Screen.* 14, 853–8.

doi:10.1177/1087057109340314

Fyhrquist, F., Saijonmaa, O., Strandberg, T., 2013. The roles of senescence and telomere shortening in cardiovascular disease. *Nat. Rev. Cardiol.* 10, 274–283. doi:10.1038/nrcardio.2013.30

Garufi, A., Trisciuglio, D., Cirone, M., D’Orazi, G., 2016. ZnCl₂ sustains the adriamycin-induced cell death inhibited by high glucose. *Cell Death Dis.* 7, e2280. doi:10.1038/cddis.2016.178

Haase, H., Hebel, S., Engelhardt, G., Rink, L., 2006. Flow cytometric measurement of labile zinc in peripheral blood mononuclear cells. *Anal. Biochem.* 352, 222–30. doi:10.1016/j.ab.2006.02.009

Klaassen, C.D., Choudhuri, S., McKim, J.M., Lehman-McKeeman, L.D., Kershaw, W.C., 1994. In vitro and in vivo studies on the degradation of metallothionein. *Environ. Health Perspect.* 102 Suppl, 141–6.

Krouwer, V.J.D., Hekking, L.H.P., Langelaar-Makkinje, M., Regan-Klapisz, E., Post, J., 2012. Endothelial cell senescence is associated with disrupted cell-cell junctions and increased monolayer permeability. *Vasc. Cell* 4, 12. doi:10.1186/2045-824X-4-12

Lichten, L.A., Cousins, R.J., 2009. Mammalian zinc transporters: nutritional and physiologic regulation. *Annu. Rev. Nutr.* 29, 153–76. doi:10.1146/annurev-nutr-033009-083312

Lopes Pinheiro, M.A., Kamermans, A., Garcia-Vallejo, J.J., van Het Hof, B., Wiert, L., O’Toole, T., Boeve, D., Verstege, M., van der Pol, S.M., van Kooyk, Y., de Vries, H.E., Unger, W.W., 2016. Internalization and presentation of myelin antigens by the brain endothelium guides antigen-specific T cell migration. *Elife* 5.

doi:10.7554/eLife.13149

Malavolta, M., Cipriano, C., Costarelli, L., Giacconi, R., Tesei, S., Muti, E., Piacenza, F., Pierpaoli, S., Larbi, A., Pawelec, G., Dedoussis, G., Herbein, G., Monti, D., Jajte, J., Rink, L., Mocchegiani, E., 2008.

Metallothionein downregulation in very old age: a phenomenon associated with cellular senescence? *Rejuvenation Res.* 11, 455–9. doi:10.1089/rej.2008.0679

Malavolta, M., Costarelli, L., Giacconi, R., Muti, E., Bernardini, G., Tesei, S., Cipriano, C., Mocchegiani, E., 2006.

Single and three-color flow cytometry assay for intracellular zinc ion availability in human lymphocytes with Zinpyr-1 and double immunofluorescence: Relationship with metallothioneins. *Cytom. Part A* 69, 1043–1053. doi:10.1002/cyto.a.20335

Malavolta, M., Piacenza, F., Costarelli, L., Giacconi, R., Muti, E., Cipriano, C., Tesei, S., Spezia, S., Mocchegiani, E., 2007. Combining UHR-SEC-HPLC-ICP-MS with flow cytometry to quantify metallothioneins and to study zinc homeostasis in human PBMC. *J. Anal. At. Spectrom.* 22, 1193. doi:10.1039/b704577h

McCabe, M.J., Jiang, S.A., Orrenius, S., 1993. Chelation of intracellular zinc triggers apoptosis in mature thymocytes. *Lab. Invest.* 69, 101–10.

Minamino, T., Miyauchi, H., Yoshida, T., Ishida, Y., Yoshida, H., Komuro, I., 2002. Endothelial Cell Senescence in Human Atherosclerosis. *Circulation* 105.

Mocchegiani, E., Costarelli, L., Basso, A., Giacconi, R., Piacenza, F., Malavolta, M., 2013. Metallothioneins, ageing and cellular senescence: a future therapeutic target. *Curr Pharm Des.* 19, 1753–1764.

Mun, G.I., Lee, S.J., An, S.M., Kim, I.K., Boo, Y.C., 2009. Differential gene expression in young and senescent endothelial cells under static and laminar shear stress conditions. *Free Radic. Biol. Med.* 47, 291–9. doi:10.1016/j.freeradbiomed.2009.04.032

Noppe, G., Dekker, P., de Koning-Treurniet, C., Blom, J., van Heemst, D., Dirks, R.W., Tanke, H.J., Westendorp,

- R.G.J., Maier, A.B., 2009. Rapid flow cytometric method for measuring senescence associated beta-galactosidase activity in human fibroblasts. *Cytometry. A* 75, 910–6. doi:10.1002/cyto.a.20796
- Ogo, O.A., Tyson, J., Cockell, S.J., Howard, A., Valentine, R.A., Ford, D., 2015. The zinc finger protein ZNF658 regulates the transcription of genes involved in zinc homeostasis and affects ribosome biogenesis through the zinc transcriptional regulatory element. *Mol. Cell. Biol.* 35, 977–87. doi:10.1128/MCB.01298-14
- Pantsulaia, I., Ciszewski, W.M., Niewiarowska, J., 2016. Senescent endothelial cells: Potential modulators of immunosenescence and ageing. *Ageing Res. Rev.* 29, 13–25. doi:10.1016/j.arr.2016.05.011
- Patrushev, N., Seidel-Rogol, B., Salazar, G., 2012. Angiotensin II requires zinc and downregulation of the zinc transporters ZnT3 and ZnT10 to induce senescence of vascular smooth muscle cells. *PLoS One* 7, e33211. doi:10.1371/journal.pone.0033211
- Perry, D.K., Smyth, M.J., Stennicke, H.R., Salvesen, G.S., Duriez, P., Poirier, G.G., Hannun, Y.A., 1997. Zinc is a potent inhibitor of the apoptotic protease, caspase-3. A novel target for zinc in the inhibition of apoptosis. *J. Biol. Chem.* 272, 18530–3.
- Rodier, F., Muñoz, D.P., Teachenor, R., Chu, V., Le, O., Bhaumik, D., Coppé, J.-P., Campeau, E., Beauséjour, C.M., Kim, S.-H., Davalos, A.R., Campisi, J., 2011. DNA-SCARS: distinct nuclear structures that sustain damage-induced senescence growth arrest and inflammatory cytokine secretion. *J. Cell Sci.* 124, 68–81. doi:10.1242/jcs.071340
- Rudolf, E., Cervinka, M., 2011. Stress responses of human dermal fibroblasts exposed to zinc pyrithione. *Toxicol. Lett.* 204, 164–73. doi:10.1016/j.toxlet.2011.04.028
- Salazar, G., Huang, J., Feresin, R.G., Zhao, Y., Griendling, K.K., 2017. Zinc regulates Nox1 expression through a NF- κ B and mitochondrial ROS dependent mechanism to induce senescence of vascular smooth muscle cells. *Free Radic. Biol. Med.* 108, 225–235. doi:10.1016/j.freeradbiomed.2017.03.032

- Seve, M., Favier, A., Osman, M., Hernandez, D., Vaitaitis, G., Flores, N.C., McCord, J.M., Flores, S.C., 1999. The Human Immunodeficiency Virus-1 Tat Protein Increases Cell Proliferation, Alters Sensitivity to Zinc Chelator-Induced Apoptosis, and Changes Sp1 DNA Binding in HeLa Cells. *Arch. Biochem. Biophys.* 361, 165–172. doi:10.1006/abbi.1998.0942
- Soto-Gamez, A., Demaria, M., 2017. Therapeutic interventions for aging: the case of cellular senescence. *Drug Discov. Today.* doi:10.1016/j.drudis.2017.01.004
- Tomat, A.L., Costa, M. de los Á., Arranz, C.T., 2011. Zinc restriction during different periods of life: Influence in renal and cardiovascular diseases. *Nutrition* 27, 392–398. doi:10.1016/j.nut.2010.09.010
- Truong-Tran, A.Q., Ho, L.H., Chai, F., Zalewski, P.D., 2000. Cellular zinc fluxes and the regulation of apoptosis/gene-directed cell death. *J. Nutr.* 130, 1459S–66S.
- Unterluggauer, H., Hampel, B., Zwerschke, W., Jansen-Dürr, P., 2003. Senescence-associated cell death of human endothelial cells: the role of oxidative stress. *Exp. Gerontol.* 38, 1149–60.
- van Deursen, J.M., 2014. The role of senescent cells in ageing. *Nature* 509, 439–446. doi:10.1038/nature13193
- Wagner, M., Hampel, B., Bernhard, D., Hala, M., Zwerschke, W., Jansen-Dürr, P., 2001. Replicative senescence of human endothelial cells in vitro involves G1 arrest, polyploidization and senescence-associated apoptosis. *Exp. Gerontol.* 36, 1327–47.
- Xiao-Hong, D., Chang-Qin, X., Jian-Hua, H., Wen-Jiang, Z., Bing, S., 2013. Icaritin delays homocysteine-induced endothelial cellular senescence involving activation of the PI3K/AKT-eNOS signaling pathway. *Pharm. Biol.* 51, 433–40. doi:10.3109/13880209.2012.738332
- Yaguchi, T., Aida, S., Kaul, S.C., Wadhwa, R., 2007. Involvement of mortalin in cellular senescence from the perspective of its mitochondrial import, chaperone, and oxidative stress management functions. *Ann. N. Y. Acad. Sci.* 1100, 306–11. doi:10.1196/annals.1395.032

Zalewski, P.D., Forbes, I.J., Seamark, R.F., Borlinghaus, R., Betts, W.H., Lincoln, S.F., Ward, A.D., 1994. Flux of intracellular labile zinc during apoptosis (gene-directed cell death) revealed by a specific chemical probe, Zinquin. *Chem. Biol.* 1, 153–61.

Zhu, Y., Tchkonja, T., Pirtskhalava, T., Gower, A.C., Ding, H., Giorgadze, N., Palmer, A.K., Ikeno, Y., Hubbard, G.B., Lenburg, M., O'Hara, S.P., LaRusso, N.F., Miller, J.D., Roos, C.M., Verzosa, G.C., LeBrasseur, N.K., Wren, J.D., Farr, J.N., Khosla, S., Stout, M.B., McGowan, S.J., Fuhrmann-Stroissnigg, H., Gurkar, A.U., Zhao, J., Colangelo, D., Dorronsoro, A., Ling, Y.Y., Barghouthy, A.S., Navarro, D.C., Sano, T., Robbins, P.D., Niedernhofer, L.J., Kirkland, J.L., 2015. The Achilles' heel of senescent cells: from transcriptome to senolytic drugs. *Aging Cell* 14, 644–58. doi:10.1111/accel.12344

Figure Legends

Figure 1. The effect of culture at an extracellular Zn concentration of 50 μ M on growth and senescence of HCAECs. Cells were passaged serially every 6-7 d and counted before re-seeding. All data are for n=6 independent cell populations for each condition (control and Zn-treated). Panel A: Cumulative population doubling (CPD) were calculated using the formula $3.32 * (\log_{10}F - \log_{10}I)$ over consecutive population doublings. Panel B: Senescence-associated β -galactosidase (SA- β -gal) activity for cells grouped by passage number and Zn treatment as indicated. Data are means with error bars showing SEM. *P<0.05 compared with passage 5-6; § P<0.05 compared with corresponding control. Panel C: p16 transcript abundance relative to GAPDH for cells grouped by passage number and Zn treatment as indicated. Data are means with error bars showing SEM. *P<0.05 compared with passage 5-6; § P<0.05 compared with corresponding control.

Figure 2. Measurements of labile Zn with FluoZin3-AM in control and Zn-treated HCAECs over the replicative lifespan using flow cytometry. Representative examples of dot plots (panels A and B) illustrating the gates set to discriminate between larger cells with features of senescent cells ("L-HCAEC") and smaller (non-large) cells ("nL-HCAEC"). Panel A: representative dot plot of control cells at passage 7 (left) and at passage 10 (right). The respective cell population doublings (CPD) and the percentage of cells in the L-HCAEC sub-population within the gate are stated above each panel. Panel B: representative dot plot of Zn treated cells at passage 7 (left) and at passage 10 (right). Panel C: Correlation between the percentage of cells in the L-HCAEC sub-population and cumulative population doublings (CPD). R^2 for controls and Zn treated cells are stated at the right of panel C. For both correlations, $p < 0.05$ by parametric (Pearson) and non-parametric (Spearman) correlation tests. Panel D: Histogram of measurements using FluoZin3-AM in the gate "nL-HCAEC". Panel E: Histogram of measurements using FluoZin3-AM in the gate "L-HCAEC". The measurement of intracellular labile Zn with FluoZin3-AM (labelled M1) requires the additional measurement of the minimum fluorescence by the membrane permeable Zn chelator TPEN (F min, labelled M3) and the maximum fluorescence (F max, labelled M4) by the Zn ionophore pyrithione. Labile Zn is then estimated using the formula $10 * (F - F \text{ min}) / (F_{\text{max}} - F)$.

Figure 3. Changes in labile Zn in HCAECs over increasing cumulative population doublings (CPDs) measured by flow cytometry with FluoZin-3-AM. Panel A: Changes in labile Zn with increasing CPDs in ungated HCAECs in control cells and cells exposed to 50 μ M Zn. Panel B: Changes in labile Zn with increasing CPDs in the gate “nL-HCAEC”; Panel C: Changes in labile Zn with increasing CPDs in the gate “L-HCAEC”. Panel D: Changes in labile Zn in cells in the gate “nL-HCAEC” grouped by cumulative population doublings (CPD), as shown. Panel E: Changes in labile Zn cells in the gate “L-HCAEC” grouped by cumulative population doublings (CPD), as shown. Significant changes were analysed by mixed models for repeated measures with SPSS 22.0. Significance of each single factor (Zn and CPD) and their interaction (int.) is shown above the graph where appropriate. Post-hoc analysis was performed by LSD. * $p < 0.05$ vs the respective measurement in the gate “nL-HCAEC”; ** $p < 0.01$ vs the respective measurement in the gate “nL-HCAEC”; ^a $p < 0.05$ compared with CPD 1-6 within the same treatment; ^b $p < 0.05$ compared to CPD 7-11 within the same treatment.

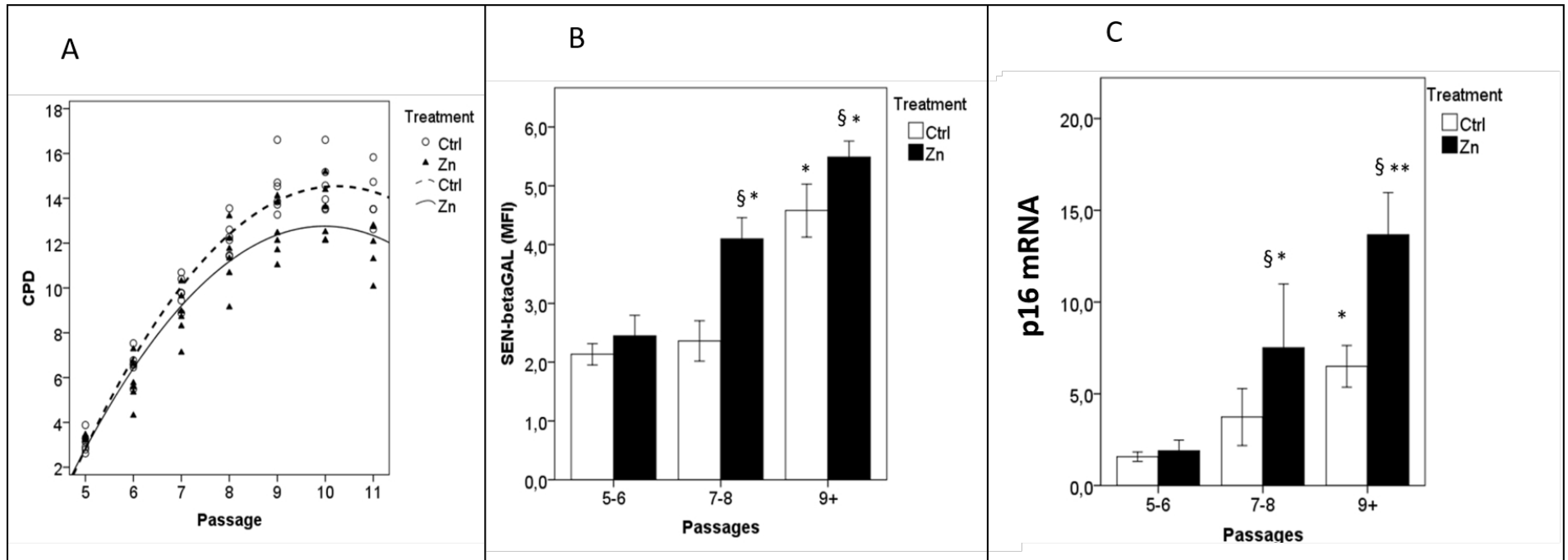
Figure 4. Imaging flow cytometry analysis of Lysotracker red and colocalization with FLuoZin-3 fluorescence in late-passage (passage 10) and early-passage (passage 5) human coronary artery endothelial cells (HCAECs). Panel a: fluorescence intensity of Lysotracker in all focused single cells (gate “all cells”), and gates “nL-HCAEC” (width $< 28 \mu$ M) and “L-HCAEC” (width $\geq 28 \mu$ M). Bars represent means with SD for 4 independent replicates. Statistical analysis was performed by ANOVA with LSD as the post-hoc test. * $p < 0.05$ vs passage 5 ** $p < 0.01$ vs passage 5; ^a $p < 0.05$ vs all cells, ^b $p < 0.05$ vs gate “nL-HCAEC”. Panel b: Representative histogram of Lysotracker fluorescence intensity in cells at passage 5. Panel c: Representative histogram of Lysotracker fluorescence intensity in cells at passage 10. Panel d: Colocalization by bright detail similarity of FluoZin-3 and Lysotracker fluorescence in all focused single cells (gate “all cells”), and the gates “nL-HCAEC” and “L-HCAEC”. Comparisons and statistics are as for panel a. Panel e: Representative histogram of bright detail similarity in cells at passage 5. Panel f: representative histogram of bright detail similarity in cells at passage 10. Panel g: Representative images of FluoZin-3 (Ch02), Lysotracker (Ch03) and overlay (Ch02/Ch03) at passage 5 showing relatively low FluoZin-3 and lysotracker staining but high colocalization (yellow area in the overlay) in cells selected from the gates “nL-

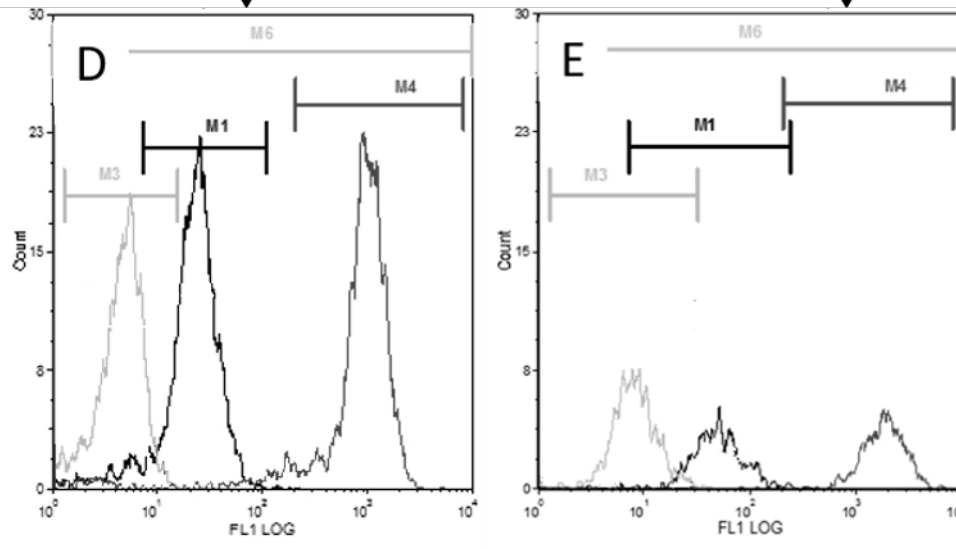
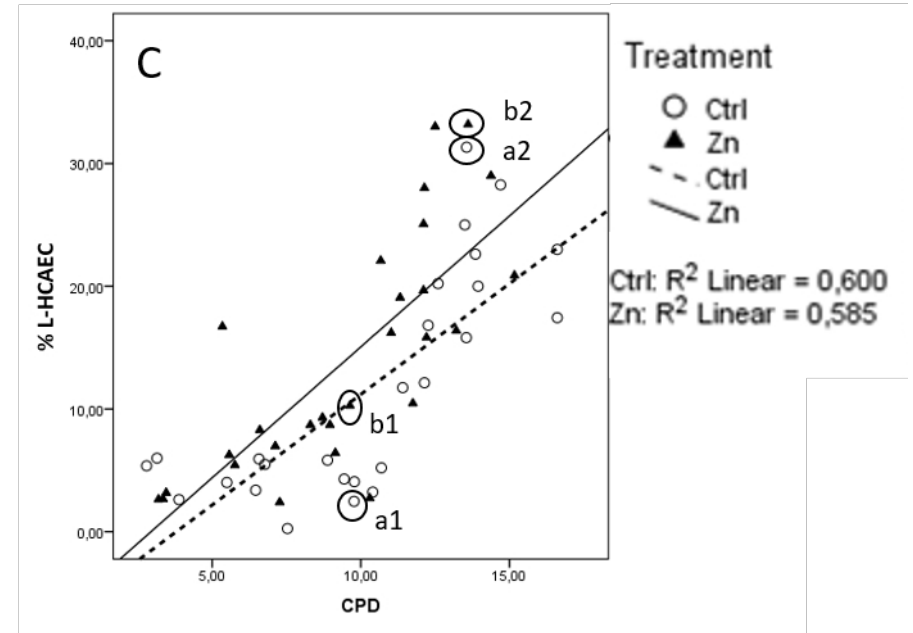
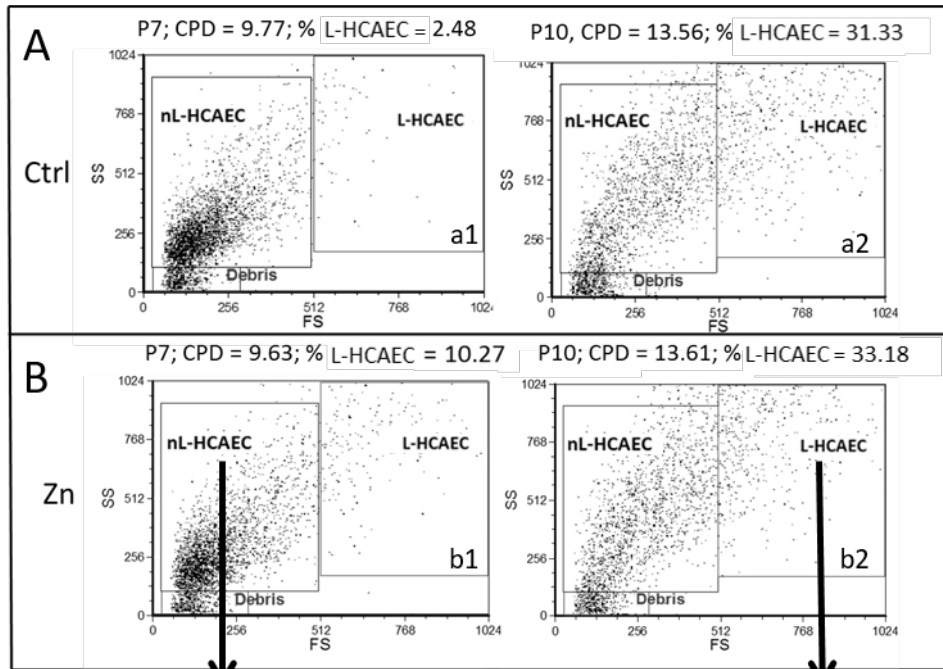
HCAEC” and “L-HCAEC”. Panel h: Representative images of Fluozin-3 (Ch02), LysoTracker (Ch03) and overlay (Ch02/Ch03) in senescent cells (passage 10) showing relatively high Fluozin-3 and LysoTracker staining but low colocalization (yellow area in the overlay) in cells selected from the gates “nL-HCAEC” and “L-HCAEC”.

Figure 5. The effect of chronic treatment with an extracellular Zn concentration of 50 μ M on the expression of a pool of Zn-sensitive genes that are involved in the regulation of Zn homeostasis (SLC30A1, SLC39A6, SLC30A5, SLC30A10, ZNF658, CBWD, SLC39A1, SLC39A2, SLC39A3, MT2A, MT1X and MT1F) analysed by RT-PqCR. Data are grouped into 3 groups according to cumulative population doublings (CPDs): early (≤ 6 CPDs), intermediate (7-11 CPDs) and late (>11 CPDs) and are means with error bars showing SEM from 3 to 5 independent experiments. Significant changes were analysed by mixed models for repeated measures with SPSS 22.0. Significance of each single factor (Zn and CPD) and their interaction (int.) is shown above the graphs. Post-hoc analysis (only to show difference based on CPDs) was performed by LSD. ^ap < 0.05 compared with CPD 1-6 within the same treatment; ^bp < 0.05 compared with CPD 7-11 within the same treatment.

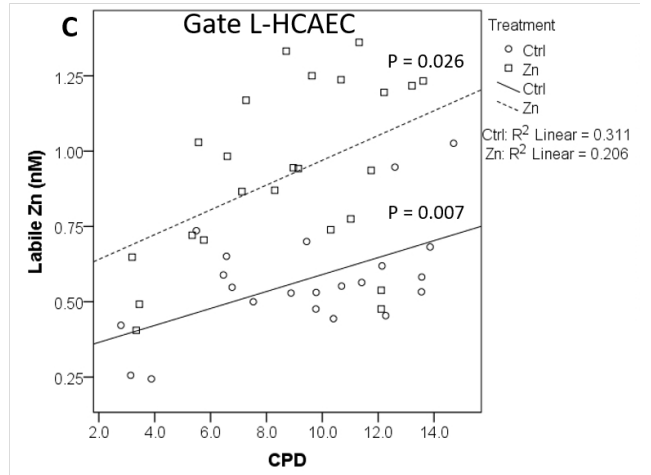
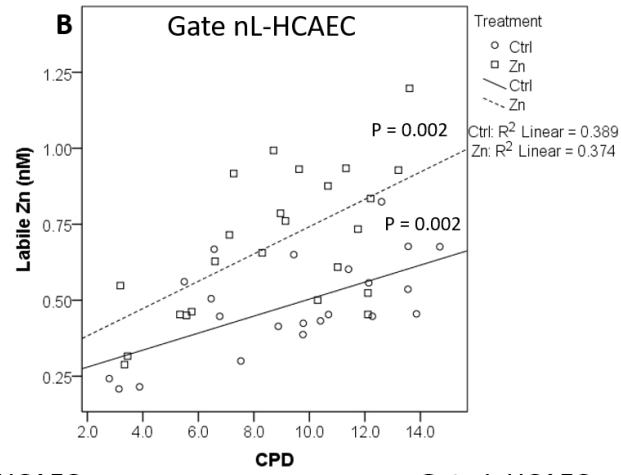
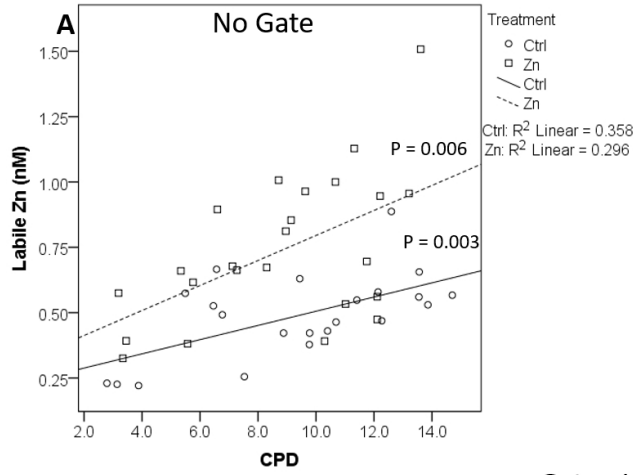
Figure 6. Effect of a short treatment (48h) with increasing doses of Zn and of the zinc chelator TPEN on the viability (measured by imaging flow cytometry with propidium iodide) of HCAECs at early-passage (passage 5) and late-passage (passage 10). Panel A: viability of cells at passage 5 with increasing doses of TPEN. Panel B: viability of cells at passage 5 with increasing doses of Zn. Panel C: viability of cells at passage 10 with increasing doses of TPEN; Panel D: viability of cells at passage 10 with increasing doses of Zn. Data are means, with bars showing SE. Statistical analysis was performed by Mixed Models with LSD as the post-hoc test. Letters representing significant differences are shown above the error bars and below the error bars for the gates “nL-HCAEC” and “L-HCAEC”, respectively. ^a p < 0.05 vs 500 nM for TPEN treatments or vs 150 μ M for Zn treatments; ^b p < 0.05 vs 100 nM for TPEN treatments or vs 100 μ M for Zn treatments; * p < 0.05 for the comparison between the gates “nL-HCAEC” and “L-HCAEC” at the specified concentration.

Figure 7. Schematic diagram to represent the effect of zinc concentration (depletion through to excess) on replicating (represented only by “non large HCAEC”) and senescent (mostly, but not exclusively, represented by “large HCAEC”) endothelial cells. The panel shading and arrow to the right indicates increasing Zn concentration (darker shading/greater width represents higher Zn concentration). Excess Zn promotes conversion of replicating cells to senescent cells and leads to death of senescent cells. Zn depletion leads to death of both replicating and senescent cells. However, senescent cells (with both “large” and “non large” morphology) are more resistant to Zn depletion than replicating cells.



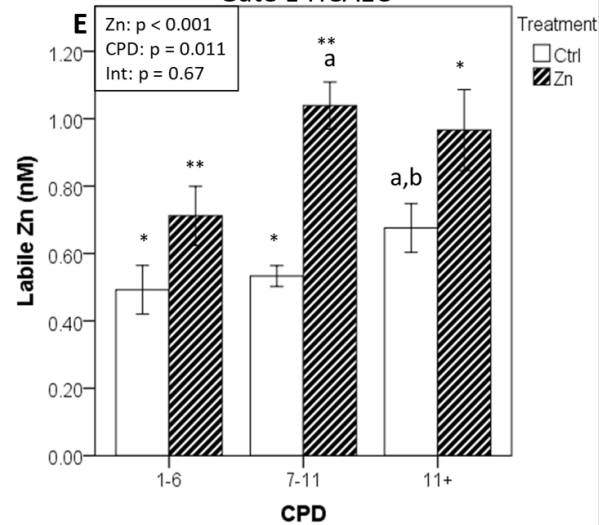
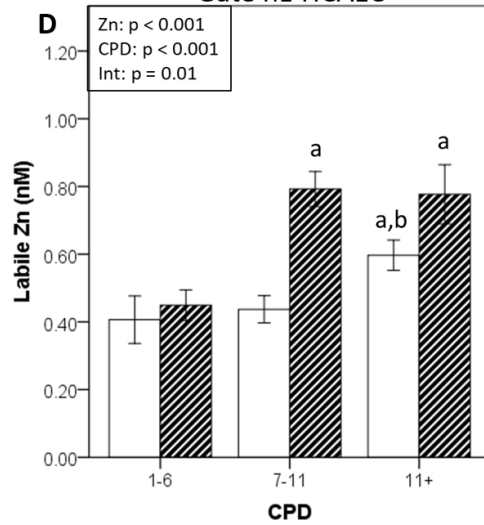


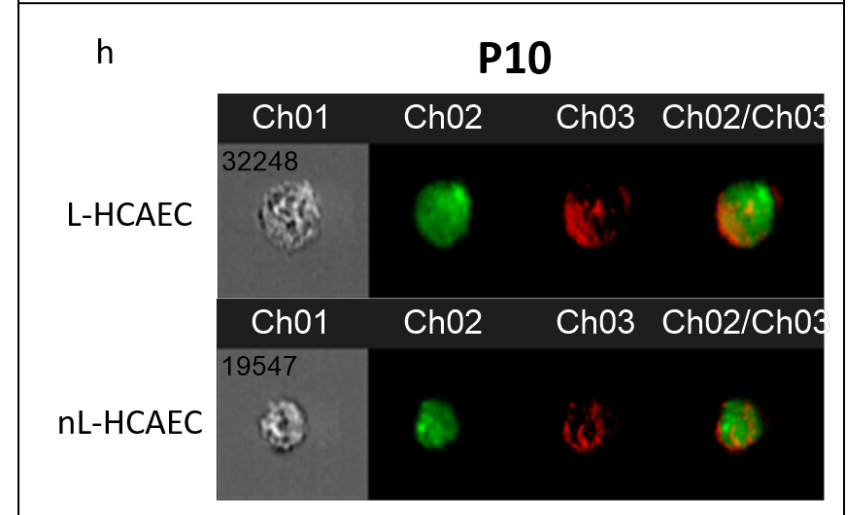
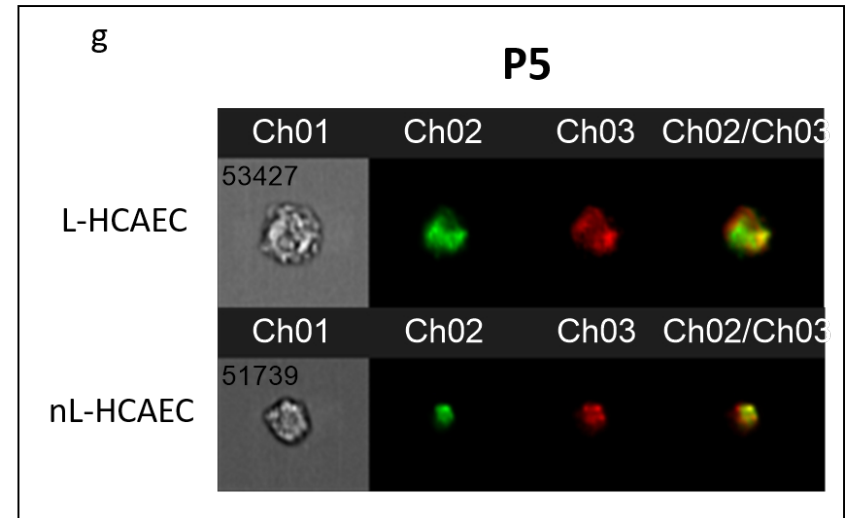
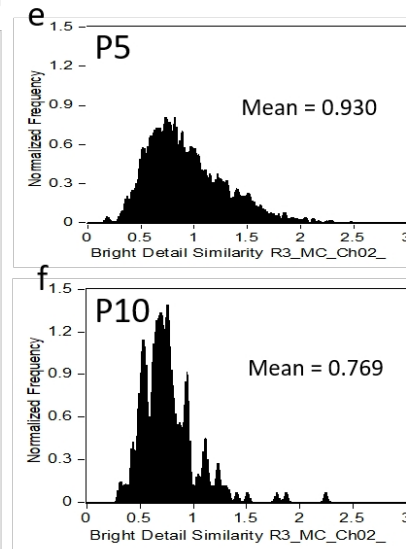
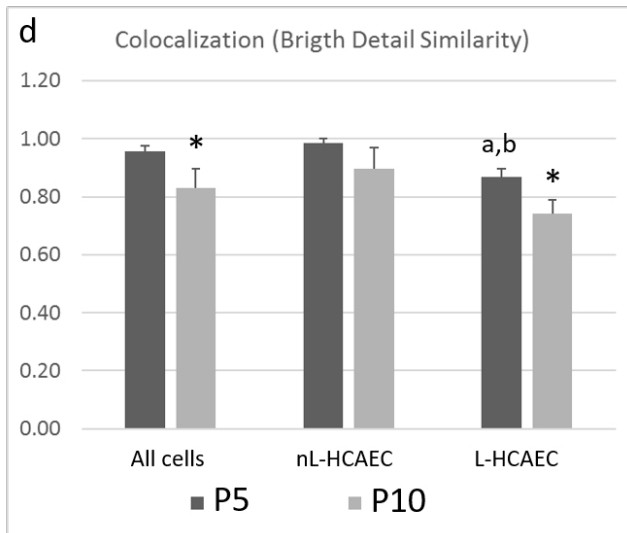
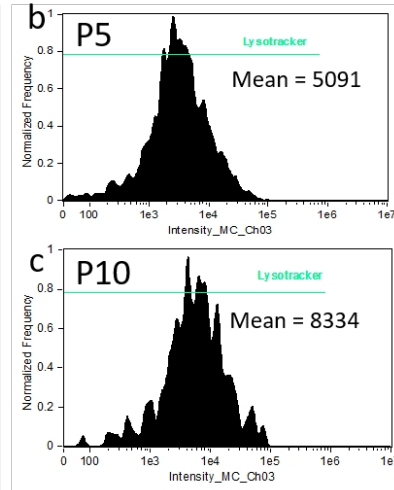
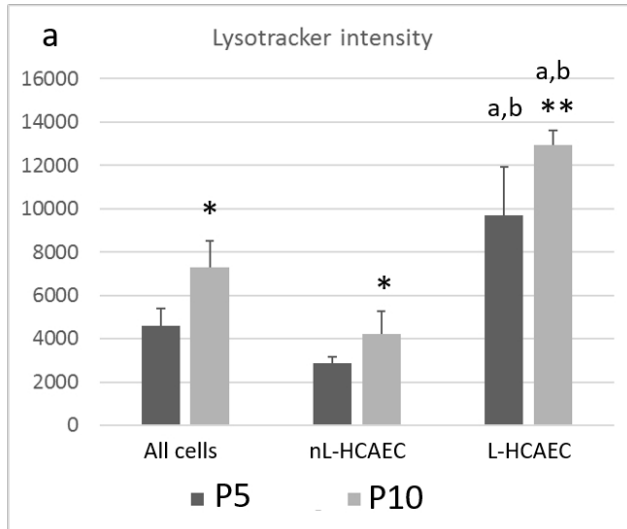
- Fluoazin3-AM (M1)
- Fluoazin3-AM + TPEN (M3)
- Fluoazin3-AM + Zn-Pyrithione (M4)

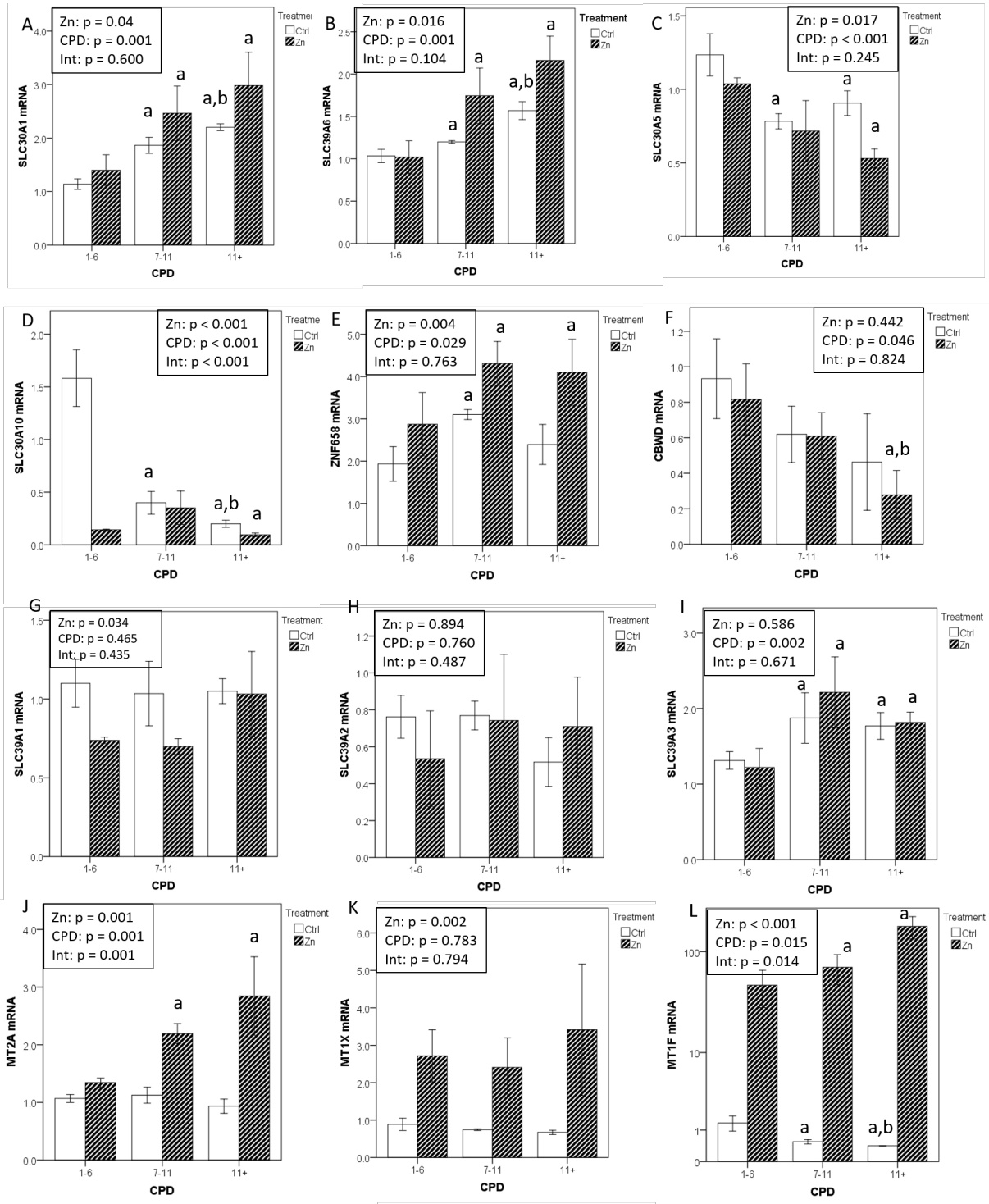


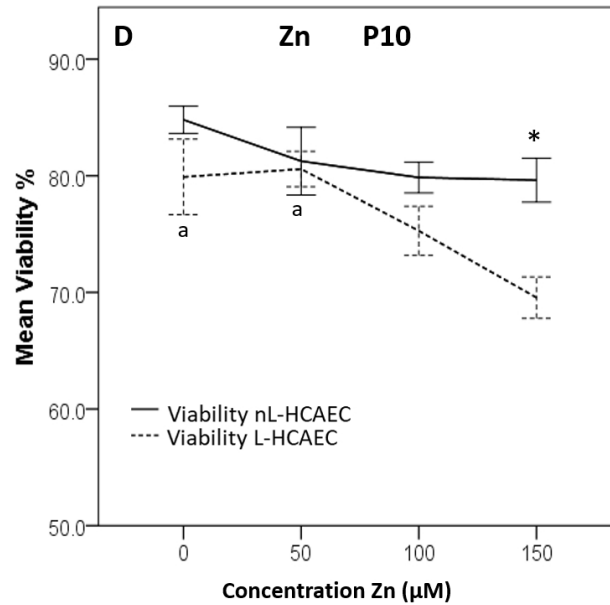
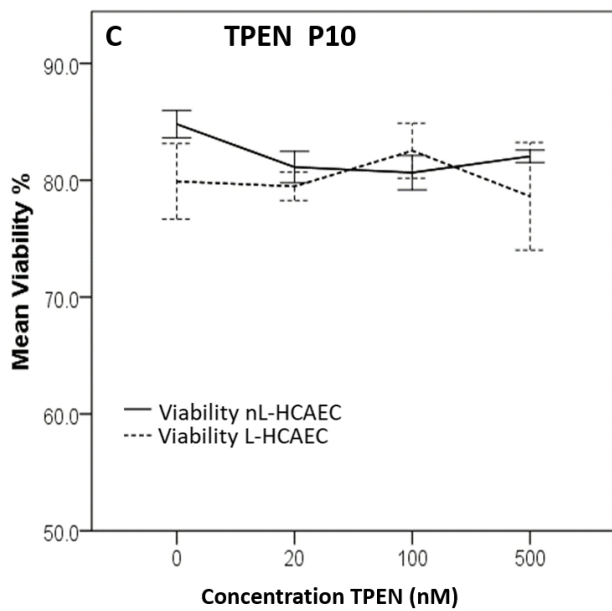
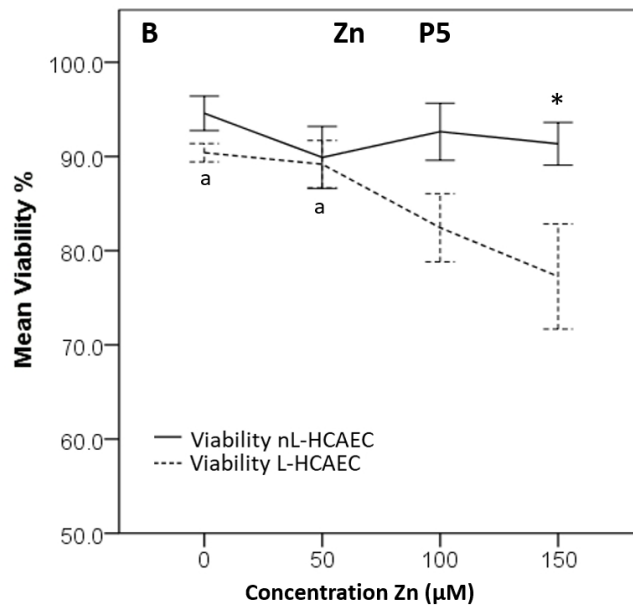
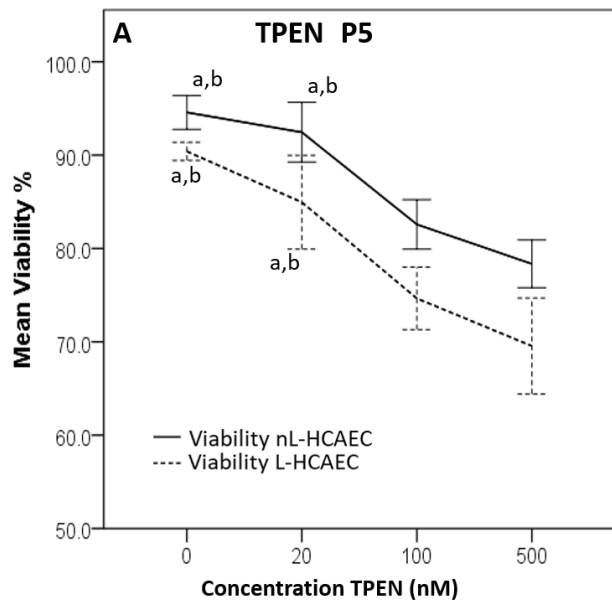
Gate nL-HCAEC

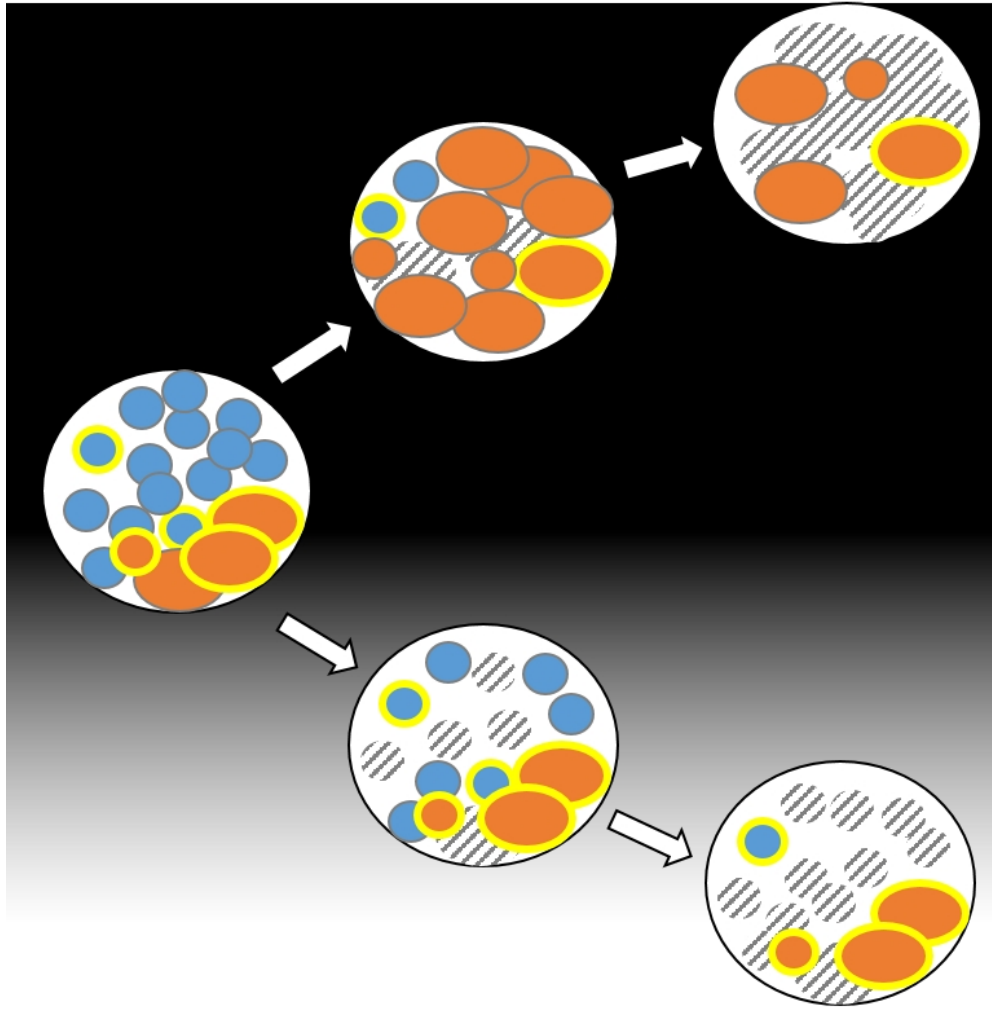
Gate L-HCAEC


















Key

Non Large HCAEC	Large HCAEC
--------------------	----------------

-  Replicating cell
-   Senescent cell
-   Subpopulations resistant to Zn depletion
-   Dead cells

[Zn]

Table 1. Cumulative population doublings and **viability of Zn-treated and **control** HCAECs**

Passage	Cumulative PD (Mean ± EM)		Viability % (Mean ± EM)	
	Ctrl	Zn	Ctrl	Zn
5,00	3.10 ± 0.18	3.32 ± 0.03	88.67 ± 1.73	89.42 ± 1.06
6,00	6.57 ± 0.27	5.81 ± 0.42	91.60 ± 1.05	<u>85.73 ± 1.39*</u>
7,00	9.83 ± 0.27	8.84 ± 0.45	82.35 ± 1.59	83.43 ± 0.64
8,00	12.24 ± 0.32	11.38 ± 0.57	81.88 ± 1.65	81.73 ± 0.85
9,00	14.45 ± 0.48	<u>12.54 ± 0.50*</u>	77.07 ± 2.77	<u>67.01 ± 1.71*</u>
10,00	14.56 ± 0.49	<u>13.32 ± 0.52*</u>	72.72 ± 4.24	70.18 ± 3.53
≥11,00	14.04 ± 0.56	<u>11.79 ± 0.51*</u>	58.48 ± 2.04	<u>14.84 ± ND#</u>

* p < 0.05 with respect to Ctrl; # **Viable** cells were not detectable in 5 of 6 cultures of Zn-treated cells

Table 2. Genes regulating Zn homeostasis that are significantly different between early and later passages of endothelial cells and show changes in the same direction

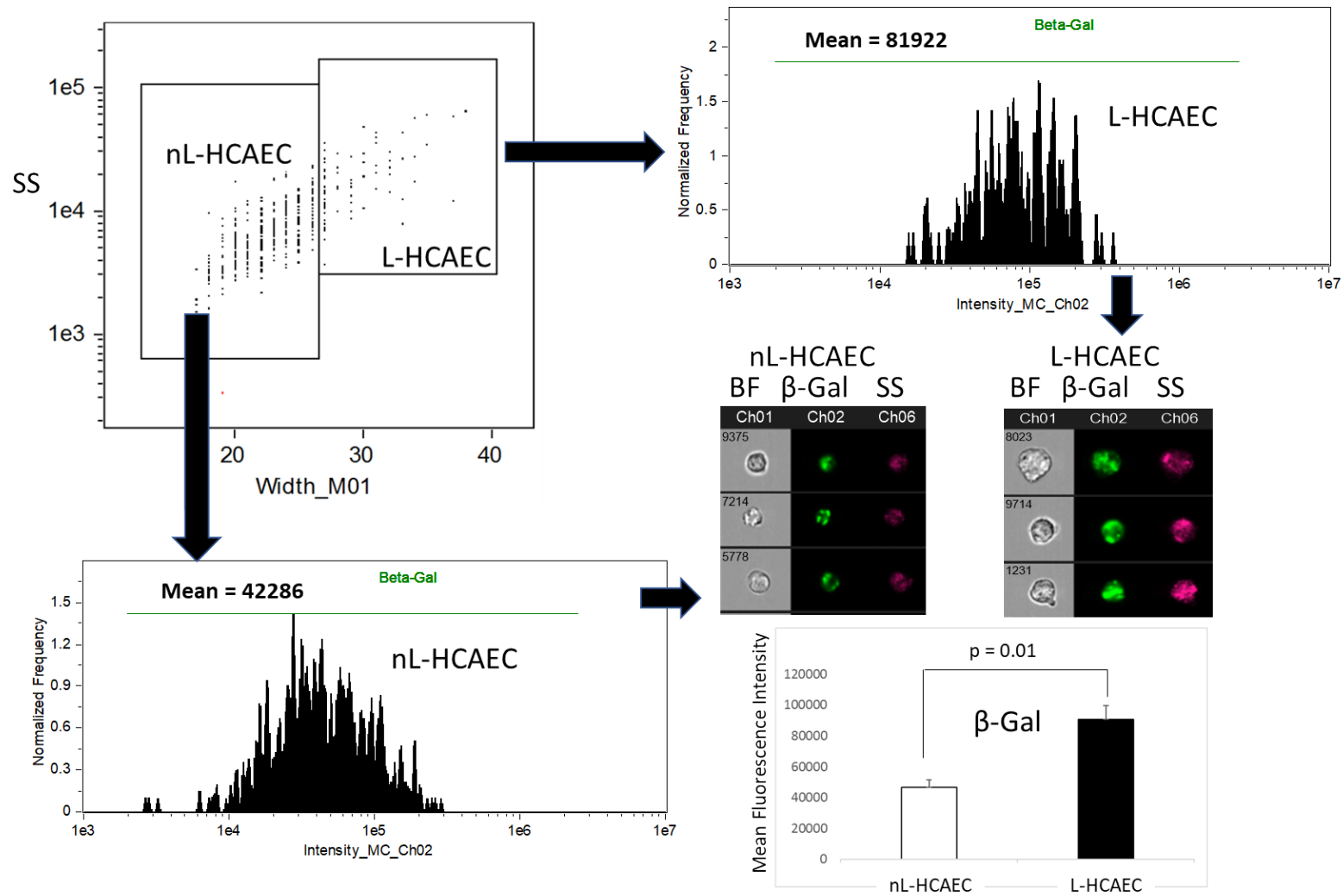
<i>Gene Symbol</i>	<i>Probesets</i>	<i>Gene Title</i>	<i>p-value</i>	<i>Fold-Change</i>	<i>p-value (HCAEC)</i>	<i>Fold-Change (HCAEC)</i>	<i>p-value (HUVEC)</i>	<i>Fold-Change (HUVEC)</i>
SLC30A1	228181_at	solute carrier family 30 (zinc transporter), member 1	2.45E-05	3.03407	5.48E-05	4.07213	0.001996	2.26062
SLC30A1	212907_at	solute carrier family 30 (zinc transporter), member 1	3.05E-08	2.47863	4.50E-08	3.39421	1.16E-05	1.81003
SLC39A6	1556551_s_at	solute carrier family 39 (zinc transporter), member 6	2.33E-05	1.68244	0.000634	1.57895	0.000122	1.79271
SLC39A13	225277_at	solute carrier family 39 (zinc transporter), member 13	0.00016	1.47173	0.000118	1.76951	0.039139	1.22407
MTF1	205323_s_at	metal-regulatory transcription factor 1	9.23E-05	1.43876	0.010151	1.26997	0.000132	1.62999
SLC39A6	202088_at	solute carrier family 39 (zinc transporter), member 6	0.000132	1.38717	0.000552	1.45406	0.003251	1.32336
SLC39A7	202667_s_at	solute carrier family 39 (zinc transporter), member 7	0.001235	1.31245	0.028535	1.23412	0.002892	1.39575
SLC39A6	202089_s_at	solute carrier family 39 (zinc transporter), member 6	0.001631	1.25043	0.023935	1.20766	0.005198	1.29471
SLC30A6	226161_at	solute carrier family 30 (zinc transporter), member 6	0.000629	-1.44044	0.003033	-1.49029	0.008364	-1.39226

Supplementary Material

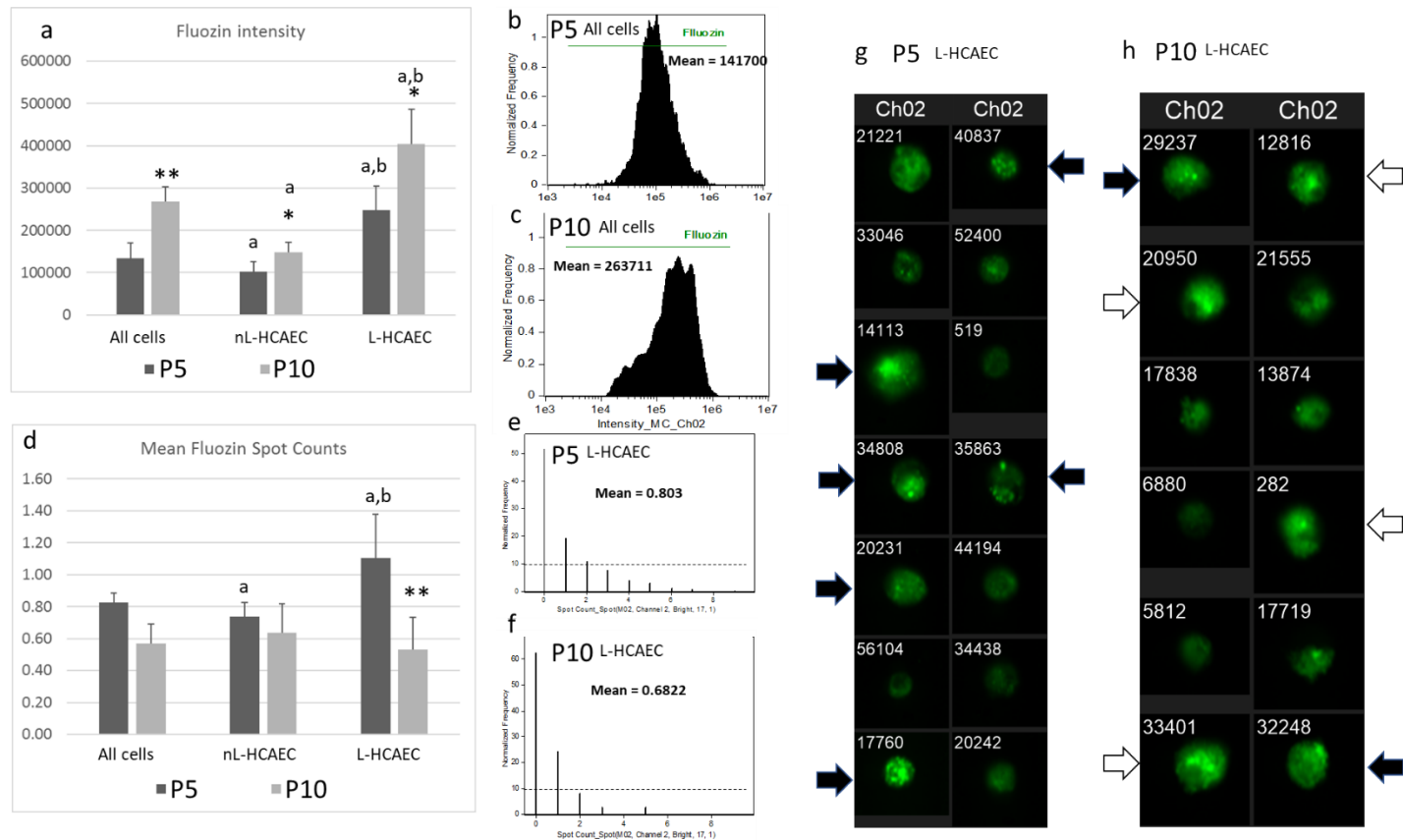
Suppl. Table 1. Primer sequences used in RT-PCR

	Forward Primer	Reverse Primer
β-actin	5'-GGATAGCACAGCCTGGATAG-3'	5'-GCGAGAAGATGACCCAGATC-3'
P-16	5'- GAG CAG CAT GGA GCC TTC -3'	5'-GCGAGAAGATGACCCAGATC-3'
ZNF658	5'-GCTGCGCACCTGGGCTGAAC-3'	5'-CCCGGGTGAATTCACAGTCACG-3'
MT1F	5'-AGTCTCTCCTCGGGTTGC-3'	5'-ACATCTGGGAGAAAGGTTGTC-3'
MT1X	5'-TCTCCTGCCTCGAAATGGAC-3'	5'-GGGCACACTTGGCACAGC-3'
MT2A	5'-GCTCCTGCAAATGCAAAGAGTG-3'	5'-CTTGTCCGACGCCCTTT-3'
SLC39A1	5'-GCCTAAAGGGAGGGGTAAGCG-3'	5'-AGTGGCGGGGACAGACC-3'
SLC39A2	5' GTTTGCCCTGTTGGCTCTCA-3'	5'ATCAATCTGGAACCATTTGAAGC-3'
SLC39A3	5'-GTTTCTGGCCACGTGCTT-3'	5'-AGGCTCAGGACCTTCTGGA-3'
SLC39A6	5'- TCT GTC TGC TGG GTC CTG TTG -3'	5'- CAG TCA CAG CCA GCG CTA CTC -3'
SLC30A1	5'-GAAAACCCAGAAAGTGGTGA-3'	5'-ATCACTGAACCCAAGGCATC-3'

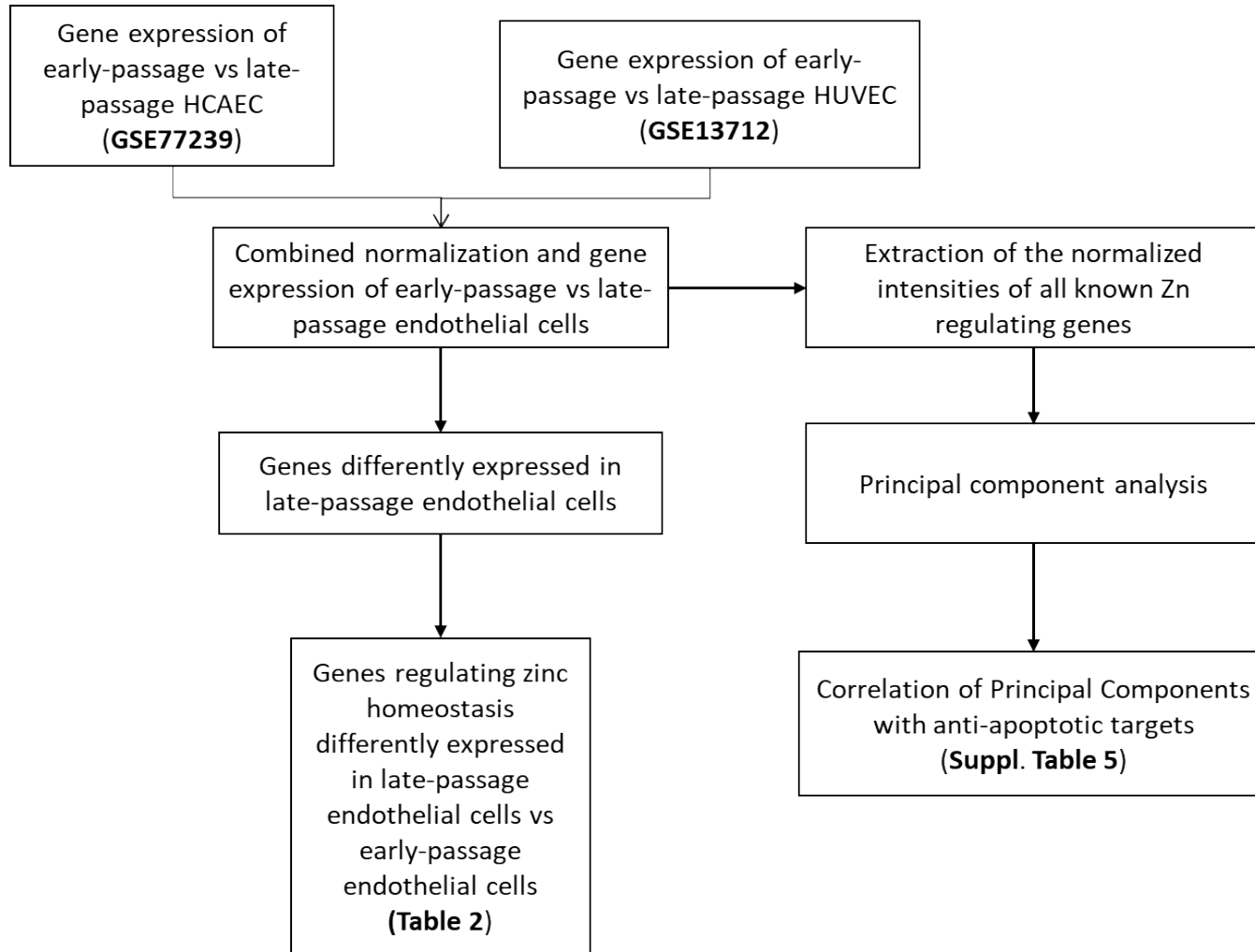
Suppl. Fig. 1. SA- β -gal staining in endothelial cells according to morphology detected by imaging flow cytometry (high width and high SS). Statistical comparison (reported in the lower right panel) of SA- β -gal between gates “nL-HCAEC” and “L-HCAEC” was performed between 3 independent replicates.



Suppl. Fig. 2. Imaging flow cytometry analysis of labile Zn stained with FluoZin-3 in late-passage (passage 10) and early-passage (passage 5) human coronary artery endothelial cells (HCAECs). Panel a: fluorescence intensity of fluozin-3 in all focused single cells (gate “all cells”), and gates “nL-HCAEC” (width < 28 μM) and “L-HCAEC” (width ≥ 28 μM). Bars represent means with SD of 4 independent replicates. Statistical analysis was performed by ANOVA with LSD as the post-hoc test; * p < 0.05 vs passage 5; ** p < 0.01 vs passage 5; ^a p < 0.05 vs all cells, ^b p < 0.05 vs gate “nL-HCAEC”. Panel b: A representative histogram of FluoZin-1 fluorescence intensity in cells at passage 5. Panel c: A representative histogram of FluoZin-1 fluorescence intensity in cells at passage 10. Panel d: Fluorescence spot counts after staining with FluoZin-3 in all focused single cells (gate “all cells”), and gates “nL-HCAEC” and “L-HCAEC”. Comparisons and statistics are as for panel a. Panel e: Representative histogram of FluoZin-3 spot counts in cells at passage 5. Panel f: representative histogram of FLuoZin-3 spot counts in cells at passage 10. Panel g: Images of FluoZin-3 spots in cells at passage 5. Cells with a high number of spots are marked by a black arrow. Panel h: Images of FluoZin-3 spots in cells at passage 10. Cells with a high number of spots are marked by a black arrow while cells with a diffuse high fluorescence are marked by white arrows.



Suppl. Figure 3. Workflow of the transcriptomic study.



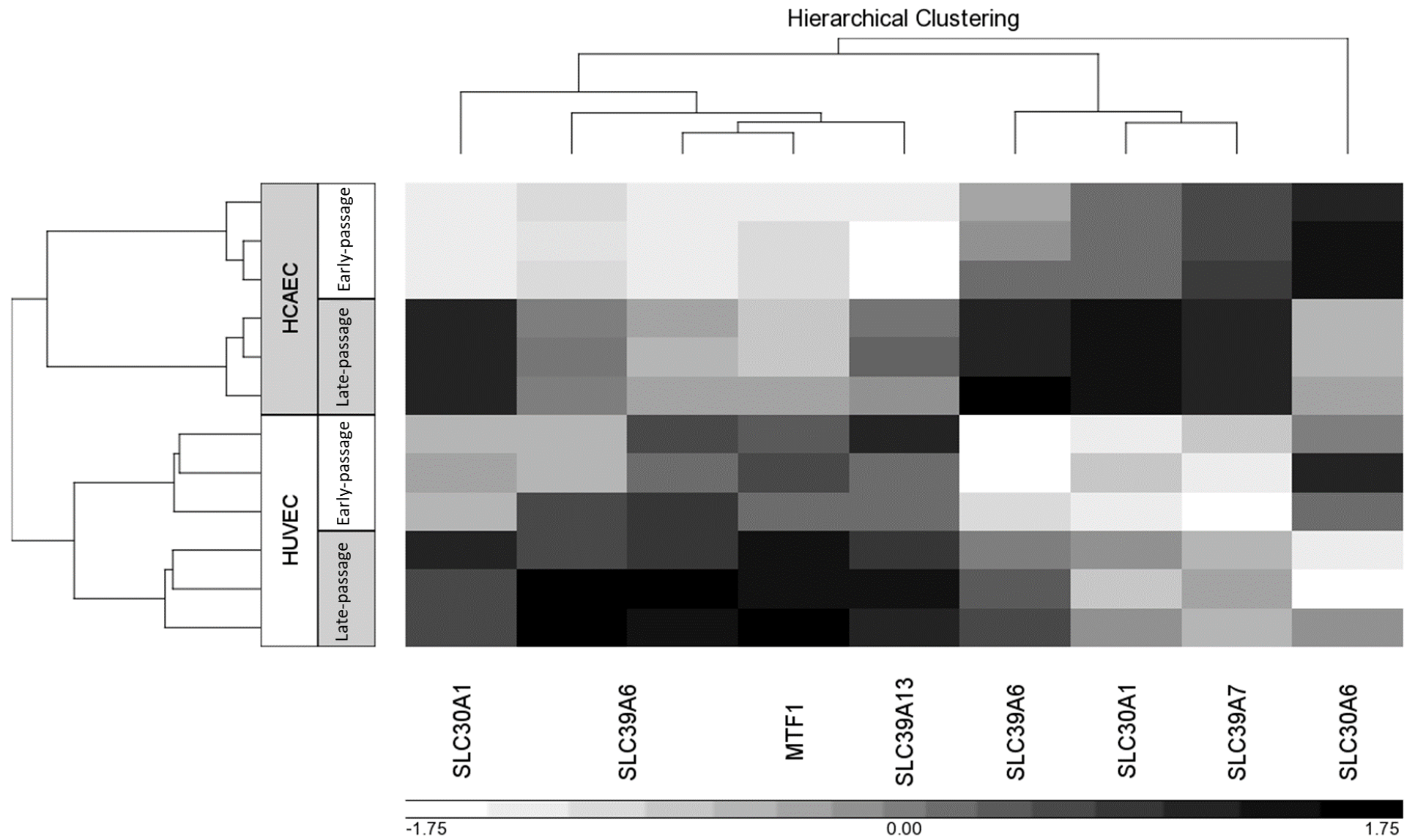
Suppl. Table 2. Genes regulating Zn homeostasis significantly **different** (FDR < 0.05) **between early and late passages** in HCAEC

<i>Gene Symbol</i>	Gene Title	p-value (HCAEC)	Fold-Change (HCAEC)
<i>SLC30A1</i>	solute carrier family 30 (zinc transporter), member 1	5.48E-05	4.07213
<i>SLC30A1</i>	solute carrier family 30 (zinc transporter), member 1	4.50E-08	3.39421
<i>SLC39A6</i>	solute carrier family 39 (zinc transporter), member 6	0.000633873	1.57895
<i>SLC39A13</i>	solute carrier family 39 (zinc transporter), member 13	0.000118141	1.76951
<i>SLC39A6</i>	solute carrier family 39 (zinc transporter), member 6	0.000552279	1.45406
<i>SLC39A13</i>	solute carrier family 39 (zinc transporter), member 13	1.31E-06	1.84154
<i>SLC30A7</i>	solute carrier family 30 (zinc transporter), member 7	0.000533541	-1.14389
<i>SLC39A4</i>	solute carrier family 39 (zinc transporter), member 4	0.000954008	-1.46228
<i>SLC30A5</i>	solute carrier family 30 (zinc transporter), member 5	0.00119457	-1.25757
<i>SLC30A6</i>	solute carrier family 30 (zinc transporter), member 6	0.00548478	-1.34538
<i>SLC30A6</i>	solute carrier family 30 (zinc transporter), member 6	0.00303293	-1.49029

Suppl. Table 3. Genes regulating Zn homeostasis significantly **different (FDR < 0.05) between early and late passages** in HUVEC

Gene Symbol	Gene Title	p-value (HUVEC)	Fold-Change (HUVEC)
SLC30A1	solute carrier family 30 (zinc transporter), member 1	0.00199595	2.26062
SLC30A1	solute carrier family 30 (zinc transporter), member 1	1.16E-05	1.81003
MT1F	metallothionein 1F	0.00499234	2.57998
SLC39A6	solute carrier family 39 (zinc transporter), member 6	0.000121869	1.79271
MT1X	metallothionein 1X	0.00719994	2.62906
MT1E	metallothionein 1E	0.00923463	2.13681
MTF1	metal-regulatory transcription factor 1	1.91E-07	2.35995
MTF1	metal-regulatory transcription factor 1	0.000132476	1.62999
SLC39A6	solute carrier family 39 (zinc transporter), member 6	0.00325139	1.32336
SLC39A7	solute carrier family 39 (zinc transporter), member 7	0.00289226	1.39575
SLC39A6	solute carrier family 39 (zinc transporter), member 6	0.00519832	1.29471
SLC30A4	solute carrier family 30 (zinc transporter), member 4	0.013025	1.35561
SLC30A7	solute carrier family 30 (zinc transporter), member 7	1.67E-07	1.4973
SLC30A7	solute carrier family 30 (zinc transporter), member 7	0.000574516	1.38476
SLC39A4	solute carrier family 39 (zinc transporter), member 4	4.25E-05	1.82365
MT3	metallothionein 3	0.00165359	1.13695
SLC30A5	solute carrier family 30 (zinc transporter), member 5	0.00109897	1.26147
SLC30A8	solute carrier family 30 (zinc transporter), member 8	0.00610457	-1.06908
SLC39A14	solute carrier family 39 (zinc transporter), member 14	0.00255617	-1.12282
SLC39A12	solute carrier family 39 (zinc transporter), member 12	0.00287793	-1.15701
SLC30A6	solute carrier family 30 (zinc transporter), member 6	0.00836428	-1.39226
SLC30A3	solute carrier family 30 (zinc transporter), member 3	1.73E-05	-2.8836

Suppl. Fig. 4. Cluster analysis of Zn-related genes significantly different in endothelial cells at late passage compared with early passage. The relative intensity shown below the figure is normalized considering only the genes shown.



Suppl. Table 4. Correlation of PCA1 and PCA2 with Zn regulating genes (component loading)*.

Part 1	PCA		Part 2	PCA		Part 3	PCA	
	1	2		1	2		1	2
Status	,030	-.836	K_1553126_a_atSLC39A12	,886	-,091	K_217859_s_atSLC39A9	,726	-,088
Cell	,981	,122	K_1552295_a_atSLC39A13	,797	,432	K_205322_s_atMTF1	,760	,535
K_212907_atSLC30A1	,038	,720	K_225277_atSLC39A13	,797	,432	K_205323_s_atMTF1	,760	,535
K_228181_atSLC30A1	-,695	,280	K_1555433_atSLC39A14	,888	-,117	K_227150_atMTF1	,426	,118
K_242716_atSLC30A1	,493	-,332	K_1555434_a_atSLC39A14	,888	-,117	K_212859_x_atMT1E	-,198	,908
K_220435_atSLC30A10	,932	-,028	K_212110_atSLC39A14	,888	-,117	K_216336_x_atMT1E	,111	,960
K_224485_s_atSLC30A2	-,857	-,048	K_220413_atSLC39A2	,817	,047	K_217165_x_atMT1F	-,366	,892
K_230084_atSLC30A2	-,579	,247	K_232115_atSLC39A3	,831	,271	K_213629_x_atMT1F	-,366	,892
K_207035_atSLC30A3	,742	-,502	K_229677_atSLC39A3	,442	,074	K_204745_x_atMT1G	,196	,869
K_227193_atSLC30A4	,420	,711	K_223917_s_atSLC39A3	,858	,171	K_210472_atMT1G	,196	,869
K_207362_atSLC30A4	,572	,373	K_219215_s_atSLC39A4	,917	,186	K_206461_x_atMT1H	,093	,923
K_238845_atSLC30A4	,739	,083	K_231667_atSLC39A5	-,513	,180	K_211456_x_atMT1HL1	,151	,871
K_243166_atSLC30A5	-,341	-,308	K_1552281_atSLC39A5	,103	,191	K_217546_atMT1M	-,439	,617
K_220181_x_atSLC30A5	,844	,048	K_1556551_s_atSLC39A6	-,373	,857	K_208581_x_atMT1X	-,319	,888
K_1555334_s_atSLC30A5	,104	-,364	K_202088_atSLC39A6	,432	,790	K_204326_x_atMT1X	-,319	,888
K_232432_s_atSLC30A5	,104	-,364	K_202089_s_atSLC39A6	,432	,790	K_212185_x_atMT2A	,166	,910
K_218989_x_atSLC30A5	,104	-,364	K_1555460_a_atSLC39A6	,432	,790			
K_226161_atSLC30A6	,233	-,828	K_202667_s_atSLC39A7	-,937	,132			
K_243643_x_atSLC30A6	,779	-,333	K_228945_s_atSLC39A8	,574	-,315			
K_226162_atSLC30A6	,233	-,828	K_209267_s_atSLC39A8	,193	-,048			
K_226217_atSLC30A7	,103	,587	K_219869_s_atSLC39A8	,127	-,088			
K_226601_atSLC30A7	-,643	,436	K_209266_s_atSLC39A8	,193	-,048			
K_239596_atSLC30A7	-,947	-,184	K_216504_s_atSLC39A8	,713	,155			
K_1552985_atSLC30A8	,897	-,260	K_222935_x_atSLC39A8	,127	-,088			
K_239983_atSLC30A8	,932	-,107	K_222445_atSLC39A9	,726	-,088			
K_229500_atSLC30A9	,652	,353	K_217859_s_atSLC39A9	,726	-,088			
K_202614_atSLC30A9	-,626	,259	K_205322_s_atMTF1	,760	,535			
K_217778_atSLC39A1	-,221	-,422						
K_225295_atSLC39A10	,934	-,241						
K_227046_atSLC39A11	-,790	-,037						

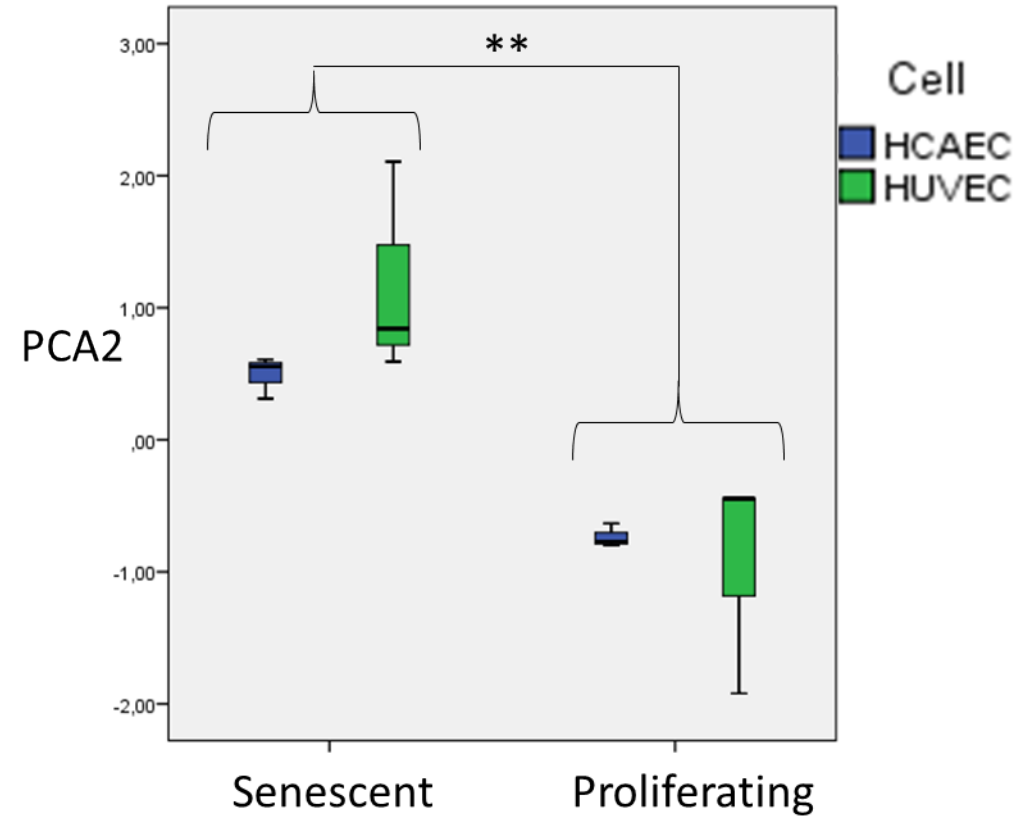
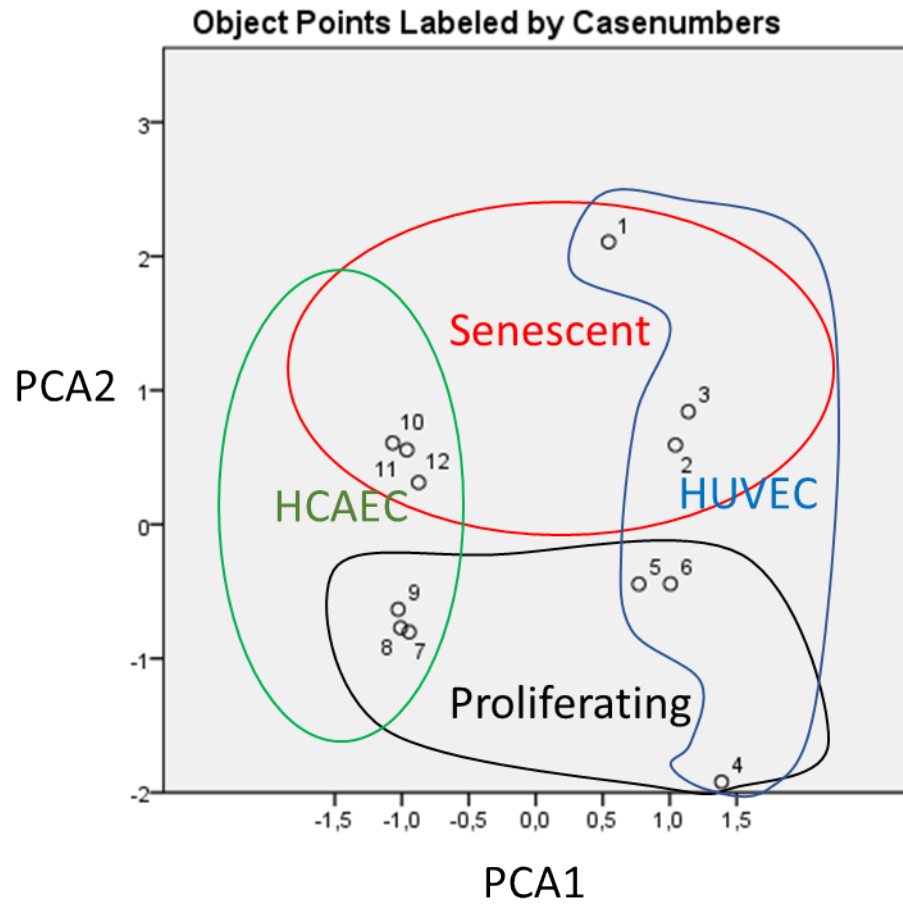
Variable Principal Normalization.

* PCA1 is associated with cell type ("Cell" in the table) while PCA2 is associated with cell status (e.g. senescent or proliferating). Each probeset contains the "K" prefix and is followed by the respective gene symbol: eg: probeset 212907_at; gene symbol: SLC30A1 is represented as K_21907_atSLC30A1. Red squares indicate correlations higher than 0.3 for PCA2.

Suppl. Table 5. Correlation of PCA2 with the intensity of genes known to exert anti-apoptotic function in senescent cells

Probeset	Gene Symbol	Spearman coeff.	Sig. (2-Tailed)	Pearson coeff.	Sig. (2-Tailed)
212312_at	BCL2L1	0.65	0.022	0.606	0.037
215037_s_at	BCL2L1	0.657	0.02	0.533	0.074
206665_s_at	BCL2L1	0.65	0.022	0.606	0.037
231228_at	BCL2L1	0.238	0.457	0.391	0.209
212190_at	SERPINE2	0.692	0.013	0.525	0.08
227487_s_at	SERPINE2	0.455	0.138	0.298	0.346
202284_s_at	CDKN1A	0.573	0.051	0.623	0.03
203879_at	PIK3CD	0.538	0.071	0.509	0.091
211230_s_at	PIK3CD	0.063	0.846	0.214	0.504
205031_at	EFNB3	-0.406	0.191	-0.352	0.261
210883_x_at	EFNB3	-0.406	0.191	-0.352	0.261
202711_at	EFNB1	0.385	0.217	0.19	0.554
202668_at	EFNB2	-0.322	0.308	-0.303	0.338
202669_s_at	EFNB2	-0.322	0.308	-0.303	0.338
202123_s_at	ABL1	0.587	0.045	0.643	0.024

Suppl. Fig. 5. Graphical representation of discriminating properties of PCA1 (cell type) and PCA2 (cell status).



Suppl. Table 6. Genes modulated by **passage number** highly correlated with PCA2.

Probeset	Gene Symbol	R	P-Value(Correlation)	Lower CI	Upper CI
222549_at	CLDN1	0.984961	5.91E-09	0.945552	0.995906
214443_at	PVR	0.965068	3.86E-07	0.876765	0.990421
228617_at	XAF1	0.955789	1.23E-06	0.845871	0.987835
209498_at	CEACAM1	0.955507	1.27E-06	0.844941	0.987756
204415_at	IFI6	0.95474	1.39E-06	0.842423	0.987542
236344_at	PDE1C	0.951913	1.87E-06	0.833178	0.986749
206133_at	XAF1	0.948735	2.56E-06	0.822865	0.985857
1557078_at	SLFN5	0.947692	2.82E-06	0.819498	0.985564
213112_s_at	SQSTM1	0.937982	6.51E-06	0.788578	0.982822
211924_s_at	PLAUR	0.934649	8.41E-06	0.778134	0.981876
220104_at	ZC3HAV1	0.933855	8.92E-06	0.775657	0.98165
207375_s_at	IL15RA	0.93381	8.95E-06	0.775518	0.981638
235705_at	---	0.932848	9.60E-06	0.772527	0.981364
209584_x_at	APOBEC3C	0.929729	1.20E-05	0.762874	0.980476
210985_s_at	SP100	0.927766	1.37E-05	0.756836	0.979916
230099_at	---	0.925945	1.55E-05	0.751264	0.979395
223159_s_at	NEK6	0.925718	1.57E-05	0.750571	0.979331
213988_s_at	SAT1	0.924776	1.67E-05	0.747698	0.979061
217165_x_at	MT1F	0.922574	1.92E-05	0.741011	0.97843
202863_at	SP100	0.917792	2.57E-05	0.726609	0.977057
204439_at	IFI44L	0.914809	3.06E-05	0.717711	0.976198
205397_x_at	SMAD3	0.914548	3.10E-05	0.716934	0.976122
202086_at	MX1	0.912756	3.43E-05	0.711623	0.975605
32699_s_at	PVR	0.910571	3.87E-05	0.705177	0.974974
206247_at	MICB	0.910294	3.93E-05	0.704361	0.974893
214444_s_at	PVR	0.905189	5.14E-05	0.689441	0.973413
202458_at	PRSS23	0.903189	5.68E-05	0.683646	0.972832
232355_at	SNORD114-3	0.899176	6.91E-05	0.672103	0.971663
204347_at	AK4 /// LOC100507855	0.896713	7.77E-05	0.665069	0.970944

202638_s_at	ICAM1	0.891281	9.94E-05	0.649704	0.969352
241347_at	RNF213	0.891274	9.94E-05	0.649685	0.96935
205899_at	CCNA1	0.885477	0.000128	0.633505	0.967645
219593_at	SLC15A3	0.885199	0.000129	0.632734	0.967563
1559883_s_at	SAMHD1	0.885031	0.00013	0.632269	0.967514
218284_at	SMAD3	0.881095	0.000153	0.621416	0.966351
202411_at	IFI27	0.880418	0.000157	0.61956	0.966151
213605_s_at	---	0.879329	0.000164	0.61658	0.965828
244778_x_at	---	0.878583	0.000169	0.614542	0.965607
207605_x_at	ZNF117	0.878472	0.00017	0.61424	0.965574
213506_at	F2RL1	0.877871	0.000174	0.6126	0.965396
240399_at	---	0.876706	0.000182	0.609432	0.965051
226702_at	CMPK2	0.874847	0.000195	0.604392	0.964498
226725_at	SLFN5	0.874634	0.000197	0.603817	0.964435
205890_s_at	GABBR1 /// UBD	0.87414	0.000201	0.602482	0.964288
243894_at	SLC41A2	0.871894	0.000218	0.596433	0.96362
209644_x_at	CDKN2A	0.87126	0.000224	0.594731	0.963431
235299_at	SLC41A2	0.870551	0.000229	0.59283	0.963219
207039_at	CDKN2A	0.868264	0.000249	0.58672	0.962537
226281_at	DNER	0.865614	0.000274	0.57968	0.961744
206542_s_at	SMARCA2	-0.86522	0.000278	-0.96163	-0.57862
208763_s_at	TSC22D3	-0.8659	0.000271	-0.96183	-0.58044
204504_s_at	HIRIP3	-0.86761	0.000255	-0.96234	-0.58498
222968_at	---	-0.87072	0.000228	-0.96327	-0.59327
225882_at	SLC35B4	-0.87151	0.000221	-0.9635	-0.59539
226085_at	CBX5	-0.87481	0.000196	-0.96449	-0.6043
225617_at	ODF2	-0.87498	0.000194	-0.96454	-0.60476
227085_at	H2AFV	-0.87694	0.00018	-0.96512	-0.61005
229513_at	STRBP	-0.87794	0.000173	-0.96542	-0.61278
218573_at	MAGEH1	-0.87904	0.000166	-0.96574	-0.61579
202179_at	BLMH	-0.87932	0.000164	-0.96583	-0.61656
225923_at	VAPB	-0.88225	0.000146	-0.96669	-0.62459

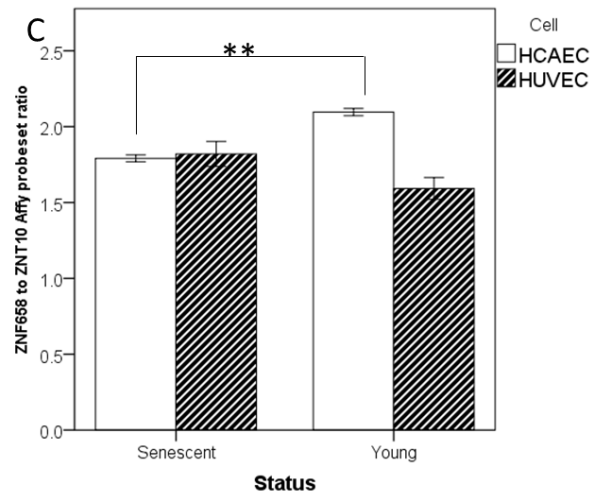
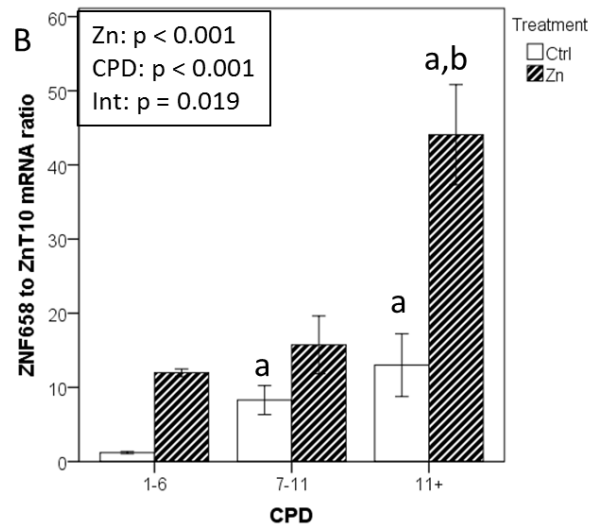
227702_at	CYP4X1	-0.88472	0.000132	-0.96742	-0.6314
225592_at	NRM	-0.88512	0.00013	-0.96754	-0.63252
227058_at	MEDAG	-0.88531	0.000129	-0.9676	-0.63303
230425_at	EPHB1	-0.88616	0.000124	-0.96785	-0.6354
230708_at	PRICKLE1	-0.88817	0.000114	-0.96844	-0.64099
201051_at	ANP32A	-0.88925	0.000109	-0.96876	-0.644
210821_x_at	CENPA	-0.89181	9.71E-05	-0.96951	-0.6512
216247_at	RPS20 /// SNORD54	-0.89261	9.37E-05	-0.96974	-0.65343
228827_at	RUNX1T1	-0.89315	9.14E-05	-0.9699	-0.65497
202457_s_at	PPP3CA	-0.89323	9.11E-05	-0.96992	-0.65519
242705_x_at	LRPAP1	-0.89385	8.86E-05	-0.97011	-0.65695
203145_at	SPAG5	-0.89407	8.77E-05	-0.97017	-0.65756
227615_at	SRRD	-0.89467	8.54E-05	-0.97035	-0.65925
217707_x_at	SMARCA2	-0.89628	7.93E-05	-0.97082	-0.66383
213264_at	PCBP2	-0.89712	7.62E-05	-0.97106	-0.66624
204875_s_at	GMDS	-0.89815	7.26E-05	-0.97136	-0.66916
211561_x_at	MAPK14	-0.89879	7.04E-05	-0.97155	-0.67098
235054_at	NUDT16	-0.89881	7.03E-05	-0.97156	-0.67107
238756_at	GAS2L3	-0.89917	6.91E-05	-0.97166	-0.67209
226879_at	HVCN1	-0.90027	6.56E-05	-0.97198	-0.67524
206316_s_at	KNTC1	-0.9025	5.88E-05	-0.97263	-0.68166
225400_at	TSEN15	-0.9067	4.75E-05	-0.97385	-0.69383
210561_s_at	WSB1	-0.90918	4.17E-05	-0.97457	-0.70109
228281_at	DDIAS	-0.9106	3.87E-05	-0.97498	-0.70525
201928_at	PKP4	-0.91607	2.84E-05	-0.97656	-0.72147
201038_s_at	ANP32A	-0.91756	2.61E-05	-0.97699	-0.72591
219076_s_at	PXMP2	-0.91775	2.58E-05	-0.97705	-0.72649
225817_at	CGNL1 /// LOC101930344 /// LOC101930349	-0.91955	2.32E-05	-0.97756	-0.7319
218349_s_at	ZWILCH	-0.92198	2.00E-05	-0.97826	-0.73921
226069_at	PRICKLE1	-0.92222	1.96E-05	-0.97833	-0.73995
211792_s_at	CDKN2C	-0.9248	1.67E-05	-0.97907	-0.74778
221726_at	RPL22	-0.92576	1.57E-05	-0.97934	-0.75071

225065_x_at	LRRC75A-AS1 /// SNORD49A /// SNORD49B /// SNORD65	-0.92666	1.48E-05	-0.9796	-0.75345
219427_at	FAT4	-0.92774	1.37E-05	-0.97991	-0.75676
207828_s_at	CENPF	-0.92865	1.29E-05	-0.98017	-0.75955
225276_at	GSPT1	-0.93072	1.12E-05	-0.98076	-0.76592
204633_s_at	RPS6KA5	-0.93111	1.09E-05	-0.98087	-0.76713
206544_x_at	SMARCA2	-0.93312	9.41E-06	-0.98144	-0.77337
213035_at	ANKRD28	-0.93367	9.04E-06	-0.9816	-0.77507
218383_at	HAUS4 /// MIR4707	-0.93616	7.50E-06	-0.9823	-0.78284
226065_at	PRICKLE1	-0.93628	7.43E-06	-0.98234	-0.78322
204235_s_at	GULP1	-0.9371	6.97E-06	-0.98257	-0.78582
207761_s_at	METTL7A	-0.93739	6.82E-06	-0.98265	-0.78671
225670_at	FAM173B	-0.93965	5.69E-06	-0.98329	-0.79384
228899_at	RP5-1136G13.2	-0.93976	5.65E-06	-0.98333	-0.79417
212736_at	C16orf45	-0.94137	4.94E-06	-0.98378	-0.79927
227889_at	LPCAT2	-0.94195	4.71E-06	-0.98395	-0.80112
209714_s_at	CDKN3	-0.94779	2.80E-06	-0.98559	-0.8198
228306_at	CNIH4	-0.95043	2.17E-06	-0.98633	-0.82836
235709_at	GAS2L3	-0.9505	2.15E-06	-0.98635	-0.82857
223519_at	ZAK	-0.95165	1.92E-06	-0.98668	-0.83232
201035_s_at	HADH	-0.95725	1.05E-06	-0.98824	-0.85069
1555758_a_at	CDKN3	-0.96056	7.04E-07	-0.98917	-0.86165
234975_at	GSPT1	-0.96081	6.82E-07	-0.98924	-0.86249
202580_x_at	FOXO1	-0.9701	1.79E-07	-0.99182	-0.89383
226364_at	HIP1	-0.97242	1.20E-07	-0.99246	-0.90177

Suppl. Fig. 6. ZNF658 to SLC30A10 ratio in HCAECs as CPDs increase.

A

Source	Sum of Squares	df	Mean Square	F	Sig.	Importance
Corrected Model ▼	330.962	3	110.321	33.787	.000	
ZNF658_ZnT10_transformed	121.089	1	121.089	37.085	.000	0.573
ZNF658_CBWD_transformed	72.995	1	72.995	22.356	.000	0.346
Residual	48.977	15	3.265			
Corrected Total	379.940	18				



Suppl. Fig. 7. Metallothionein protein expression. The effect of an extracellular Zn concentration of 50 μ M on MT protein expression measured by flow cytometry in HCAECs grouped according to CPD. Significant changes were analysed by mixed models for repeated measures with SPSS 22.0. Significance of each single factor (Zn and CPD) and their interaction (int.) is shown above the graphs. Post-hoc analysis (only to show difference based on CPDs) was performed by LSD. ^a $p < 0.05$ compared with CPD 1-6 within the same treatment; ^b $p < 0.05$ compared with CPD 7-11 within the same treatment.

